The factorization method for the acoustic transmission problem

Konstantinos A Anagnostopoulos[†], Antonios Charalambopoulos[‡]‖ and Andreas Kleefeld[§]

[†]Department of Informatics and Communications, Technological Educational Institute of Serres, 62124 Serres, Greece

[‡]Department of Applied Mathematics and Physical Sciences, National Technical University of Athens, 15780 Athens, Greece

[§]Department I (Mathematics, Natural Sciences, Computer Science), Brandenburgische Technische Universität, 03013 Cottbus, Germany

E-mail: k.a.anagnostopoulos@gmail.com, acharala@math.ntua.gr and kleefeld@tu-cottbus.de

Abstract. In the present work, the shape reconstruction problem of acoustically penetrable bodies from far-field data corresponding to time-harmonic plane wave incidence is investigated within the framework of the factorization method. Although the latter technique has received considerable attention in inverse scattering problems dealing with impenetrable scatterers, it has not been elaborated for inverse transmission problems with the only exception being a work by the first two authors and co-workers. Aimed at bridging this gap in the field of acoustic scattering, the paper at hand focuses on establishing rigorously the necessary theoretical framework for the application of the factorization method to the inverse acoustic transmission problem. The main outcome of the undertaken investigation is the derivation of an explicit formula for the scatterer's characteristic function, which depends solely on the far-field data feeding the inverse scattering scheme. Extended numerical examples in three dimensions are also presented, where a variety of different surfaces are successfully reconstructed by the factorization method, thus complementing the method's validation from the computational point of view.

Submitted to: *Inverse Problems*

1. Introduction

The *factorization method* is an inverse scattering technique which is placed among a wider class of non-iterative methods dealing with the *shape identification problem* of inverse scattering theory and usually referred to as *sampling methods*. The recorded literature on these methods is of great extent and we refer the interested reader to the survey articles [17, 52, 53] and the monographs [10, 16, 34]. We henceforth focus on

‖ Author to whom any correspondence should be addressed.

the factorization method, which aims at constructing a binary criterion for deciding whether a given point —from a grid of 'sampling' points in a region known in advance to contain the unknown scatterer— is inside or outside the scattering obstacle by using solely the far-field data. Thus one is able to compute an approximation to the scatterer's characteristic function with the only *a priori* information on the scatterer being a coarse estimation about its location. Stated otherwise, no *a priori* information concerning either the geometric/topological (e.g., number of connectivity components) or physical (i.e., the exact type of boundary condition(s)) properties of the scattering obstacle is necessary for the method to work. Moreover, the straightforwardness of its numerical implementation and the remarkably low computational time needed for delivering a reconstruction (even for three-dimensional applications) render the factorization method even more attractive among the large body of inverse scattering schemes. On the other hand, the fact that it requires a large amount of data, i.e., a knowledge of the far-field pattern for all directions of incidence and observation might be included in the short list of its drawbacks.

Since its first presentation by Andreas Kirsch in the original paper [28] for the shape reconstruction of an acoustically soft or hard scatterer (see, also, [14]), the factorization method has been successfully applied to other problems for the scalar Helmholtz equation including scattering by inhomogeneous media [29, 30, 31, 37], obstacles with impedance or mixed boundary conditions (see [21, 22] and the references therein), periodic surfaces with Dirichlet or Robin boundary conditions [4, 3] and arcs [38]. In addition, the method has been elaborated for various static problems [23, 46, 47, 48] while a discussion on its extension to inverse problems for general elliptic equations can be found in [19, 33]. For developments of the theory of the method for the system of Maxwell's equations we refer to [20, 32], while for solutions of elastic scattering problems via the factorization method to references [2] and [1], where the inverse scattering problem by rigid bodies or cavities is examined in a two- and three-dimensional setting, respectively, and to the study [13] for a complete investigation of the inverse elastic transmission problem. Finally, applications of the factorization method to problems in impedance and optical tomography can be found, among others, in [8, 9, 24] and [6, 25], respectively.

It has to be noted that the recorded literature on the factorization method is generally characterized by a lack of theoretical results concerning with its derivation/application to inverse scattering problems dealing with penetrable scatterers, a situation which naturally occurs in a variety of physical situations in the field of wave scattering. More precisely, to the best of our knowledge at least, the only study dealing with the solution of the inverse transmission problem via the factorization method is one of the first two authors in reference [13] for the case of an isotropic and homogeneous elastic inclusion in three dimensions. Motivated by this, the present study is devoted to the developement of a complete framework, both theoretical and numerical, which is necessary for the application of the factorization method to the problem of reconstructing the support of a homogeneous penetrable body from the

knowledge of the far-field pattern of the scattered fields for acoustic plane incident waves.

This paper is organized as follows. In section 2, we formulate the direct and inverse scattering problems and introduce the concept of the far-field operator, on which the formulation of the investigated inverse technique relies heavily. Section 3 contains the main results of this paper. Most effort there has been spent on deriving a factorization of the far-field operator, which is the cornerstone for the applicability of the specific inversion scheme, and investigating thorougly the properties of the involved operators. By means of the proposed factorization, we are then able to employ an abstract functional theoretic result (see [34] or [17, Theorem 5.4]) concerning the $(F^*F)^{1/4}$-variant of the factorization method, which finally leads to an explicit characterization of the scattering obstacle. Finally, an extended discussion of the numerical implementation of the method in three dimensions accompanied by various reconstruction examples corroborating its high performance as an inverse solver have been included in section 4.

2. Formulation of the direct and inverse scattering problem

Let $D \subset \mathbb{R}^3$ be a bounded domain with boundary ∂D of class $C^{2,\alpha}$, henceforth called the scatterer, and denote by $\hat{\boldsymbol{\nu}}$ the unit normal vector to the boundary ∂D directed into the exterior of D. The exterior $\mathbb{R}^3\backslash\overline{D}$ of the scatterer (with $\overline{D} = D \cup \partial D$), which is assumed to be connected, is an infinite homogeneous isotropic non-absorbing acoustic medium characterized by mass density ρ_e, mean compressibility κ_e and sound speed $c_\mathrm{e} = 1/\sqrt{\kappa_\mathrm{e}\rho_\mathrm{e}}$, whereas the medium occupying the interior of the scatterer D is characterized by the corresponding physical parameters ρ_i, κ_i and $c_\mathrm{i} = 1/\sqrt{\kappa_\mathrm{i}\rho_\mathrm{i}}$. The scatterer is excited by a time-harmonic acoustic plane wave u^inc of unit amplitude, which propagates in the direction $\hat{\boldsymbol{d}} \in \Omega$, where $\Omega := \{\boldsymbol{x} \in \mathbb{R}^3 \colon |\boldsymbol{x}| = 1\}$ is the unit sphere in $\mathbb{R}^3$ (here, $|\cdot|$ denotes the standard Euclidean norm in $\mathbb{R}^3$, while the hat on the top of a vector indicates unit length). After suppressing the harmonic time dependence $\mathrm{e}^{-\mathrm{i}\omega t}$ with $\omega \in \mathbb{R}^+$ standing for the angular frequency and $\mathrm{i} = \sqrt{-1}$, the incident wave is represented by the simple closed-form expression

$$u^\mathrm{inc}(\boldsymbol{x}; \hat{\boldsymbol{d}}) = \mathrm{e}^{\mathrm{i}k_\mathrm{e}\boldsymbol{x}\cdot\hat{\boldsymbol{d}}}, \qquad \boldsymbol{x} \in \mathbb{R}^3, \tag{1}$$

where $k_\mathrm{e} = \omega/c_\mathrm{e}$ is the wave number of the acoustic waves in the host medium.

The interference of the incident wave (1) with the penetrable scatterer leads to the creation of two secondary fields; namely, the scattered field $u^\mathrm{sct}(\boldsymbol{x}; \hat{\boldsymbol{d}})$, which is defined for $\boldsymbol{x} \in \mathbb{R}^3\backslash\overline{D}$ and propagates outwards and the transmitted field $u^\mathrm{int}(\boldsymbol{x}; \hat{\boldsymbol{d}})$, which is defined in the interior of the scattering obstacle ($\boldsymbol{x} \in D$). The total acoustic field in the exterior of the scatterer is formed by the superposition of the incident and the scattered field, i.e., $u^\mathrm{ext}(\boldsymbol{x}; \hat{\boldsymbol{d}}) = u^\mathrm{inc}(\boldsymbol{x}; \hat{\boldsymbol{d}}) + u^\mathrm{sct}(\boldsymbol{x}; \hat{\boldsymbol{d}})$, $\boldsymbol{x} \in \mathbb{R}^3\backslash\overline{D}$, and the fields u^a, $a = \{\mathrm{int}, \mathrm{ext}\}$ satisfy, in their domains of definition, the *reduced wave equation* or *Helmholtz equation*, that is,

$$\Delta u^\mathrm{int}(\boldsymbol{x}; \hat{\boldsymbol{d}}) + k_\mathrm{i}^2 u^\mathrm{int}(\boldsymbol{x}; \hat{\boldsymbol{d}}) = 0, \qquad \boldsymbol{x} \in D, \tag{2a}$$

$$\Delta u^{\text{ext}}(\boldsymbol{x};\hat{\boldsymbol{d}}) + k_{\text{e}}^2 u^{\text{ext}}(\boldsymbol{x};\hat{\boldsymbol{d}}) = 0, \qquad \boldsymbol{x} \in \mathbb{R}^3\backslash\overline{D}, \tag{2b}$$

where $\Delta \equiv \boldsymbol{\nabla}\cdot\boldsymbol{\nabla}$ is the well-known Laplace operator and $k_{\text{i}} = \omega/c_{\text{i}}$ is the wave number of the acoustic medium filling the interior of D.
The continuity of the acoustic pressure and of the normal component of the particle velocity across the interface ∂D (see [7, Section 3.1] for the complete derivation) leads to the *transmission boundary conditions*

$$u^{\text{int}}(\boldsymbol{x};\hat{\boldsymbol{d}}) = u^{\text{ext}}(\boldsymbol{x};\hat{\boldsymbol{d}}), \qquad \boldsymbol{x} \in \partial D, \tag{3a}$$

$$\frac{\partial u^{\text{int}}(\boldsymbol{x};\hat{\boldsymbol{d}})}{\partial\hat{\boldsymbol{\nu}}(\boldsymbol{x})} = \tau\frac{\partial u^{\text{ext}}(\boldsymbol{x};\hat{\boldsymbol{d}})}{\partial\hat{\boldsymbol{\nu}}(\boldsymbol{x})}, \qquad \boldsymbol{x} \in \partial D, \tag{3b}$$

where $\tau := \rho_{\text{i}}/\rho_{\text{e}} \in \mathbb{R}^+$ is the mass density ratio of the two media. In addition, the partial differential equations (2) and the boundary conditions (2) must be supplemented by the *Sommerfeld's radiation condition* (see equation (8) below) referring to the scattered field u^{sct} in order to form a well-posed boundary value problem (BVP) (see, e.g., [15]).

In mathematical terms, the secondary fields $u^{\text{int}}(\boldsymbol{x})$ and $u^{\text{sct}}(\boldsymbol{x})$ (their dependence on the propagation vector $\hat{\boldsymbol{d}}$ is omitted for simplicity) satisfy the so-called *classical acoustic transmission scattering problem*: find a pair of functions $(u^{\text{int}}, u^{\text{sct}})$ with $u^{\text{int}} \in C^2(D)\cap C^1(\overline{D})$ and $u^{\text{sct}} \in C^2(\mathbb{R}^3\backslash\overline{D})\cap C^1(\mathbb{R}^3\backslash D)$ such that

$$\Delta u^{\text{int}}(\boldsymbol{x}) + k_{\text{i}}^2 u^{\text{int}}(\boldsymbol{x}) = 0, \qquad \boldsymbol{x} \in D, \tag{4}$$

$$\Delta u^{\text{sct}}(\boldsymbol{x}) + k_{\text{e}}^2 u^{\text{sct}}(\boldsymbol{x}) = 0, \qquad \boldsymbol{x} \in \mathbb{R}^3\backslash\overline{D}, \tag{5}$$

$$u^{\text{int}}(\boldsymbol{x}) - u^{\text{sct}}(\boldsymbol{x}) = f(\boldsymbol{x}), \qquad \boldsymbol{x} \in \partial D, \tag{6}$$

$$\tau^{-1}\frac{\partial u^{\text{int}}}{\partial\hat{\boldsymbol{\nu}}}(\boldsymbol{x}) - \frac{\partial u^{\text{sct}}}{\partial\hat{\boldsymbol{\nu}}}(\boldsymbol{x}) = h(\boldsymbol{x}), \qquad \boldsymbol{x} \in \partial D, \tag{7}$$

$$\lim_{r\to\infty} r\left(\frac{\partial u^{\text{sct}}(\boldsymbol{x})}{\partial r} - \mathrm{i}k_{\text{e}}u^{\text{sct}}(\boldsymbol{x})\right) = 0, \qquad r = |\boldsymbol{x}|, \tag{8}$$

with specific data $f(\boldsymbol{x}) := u^{\text{inc}}(\boldsymbol{x})$ and $h(\boldsymbol{x}) := (\partial u^{\text{inc}}/\partial\hat{\boldsymbol{\nu}})(\boldsymbol{x})$ for $\boldsymbol{x} \in \partial D$. Equation (8), which holds uniformly over all directions $\hat{\boldsymbol{x}} = \boldsymbol{x}/r$, stands for the Sommerfeld's radiation condition. It is pointed out that a solution to (5) satisfying (8) will be called a *radiating solution* of the Helmholtz equation in $\mathbb{R}^3\backslash\overline{D}$. Finally, it is known that problem (4)–(8) constitutes a well-posed BVP [15, 45, 18]. Moreover, the specific BVP disposes also a weak formulation in which (4) and (5) are satisfied in the sense of distributions by the fields $u^{\text{int}} \in H^1(D)$ and $u^{\text{sct}} \in H^1_{\text{loc}}(\mathbb{R}^3\backslash\overline{D})$ (H^k denotes the usual Sobolev space) and (6), (7) are satisfied in the sense of the trace operator with arbitrary boundary data $(f,h) \in H^{1/2}(\partial D)\times H^{-1/2}(\partial D)$. This problem will be referred to as the *transmission problem* (TP).

Let us recall that any radiating solution $v \in C^2(\mathbb{R}^3\backslash\overline{D})\cap C^1(\mathbb{R}^3\backslash D)$ to the Helmholtz equation can be represented by the *Green's representation formula*

$$v(\boldsymbol{x}) = \int_{\partial D}\left[v(\boldsymbol{y})\frac{\partial\Phi_a(\boldsymbol{x},\boldsymbol{y})}{\partial\hat{\boldsymbol{\nu}}(\boldsymbol{y})} - \frac{\partial v}{\partial\hat{\boldsymbol{\nu}}}(\boldsymbol{y})\,\Phi_a(\boldsymbol{x},\boldsymbol{y})\right]\mathrm{d}s(\boldsymbol{y}), \qquad \boldsymbol{x} \in \mathbb{R}^3\backslash\overline{D}, \tag{9}$$

where $\Phi_a(\boldsymbol{x},\boldsymbol{y})$, $a=\{\mathrm{e},\mathrm{i}\}$ is the fundamental solution of the Helmholtz equation with wavenumber k_a, that is,

$$\Phi_a(\boldsymbol{x},\boldsymbol{y})=\frac{\mathrm{e}^{\mathrm{i}k_a|\boldsymbol{x}-\boldsymbol{y}|}}{4\pi\,|\boldsymbol{x}-\boldsymbol{y}|},\qquad \boldsymbol{x},\boldsymbol{y}\in\mathbb{R}^3,\quad \boldsymbol{x}\neq\boldsymbol{y}. \tag{10}$$

Clearly, the asymptotic behaviour of the fundamental solution (with the parameters of the exterior space, i.e., $a=\mathrm{e}$) is of the form

$$\Phi_{\mathrm{e}}(\boldsymbol{x},\boldsymbol{y})=\frac{\mathrm{e}^{\mathrm{i}k_{\mathrm{e}}|\boldsymbol{x}|}}{|\boldsymbol{x}|}\Phi_{\mathrm{e}}^{\infty}(\hat{\boldsymbol{x}},\boldsymbol{y})+\mathcal{O}(|\boldsymbol{x}|^{-2}),\qquad |\boldsymbol{x}|\to\infty, \tag{11}$$

uniformly with respect to the observation directions $\hat{\boldsymbol{x}}=\boldsymbol{x}/|\boldsymbol{x}|\in\Omega$ with

$$\Phi_{\mathrm{e}}^{\infty}(\hat{\boldsymbol{x}},\boldsymbol{y}):=\frac{1}{4\pi}\exp\{-\mathrm{i}k_{\mathrm{e}}\hat{\boldsymbol{x}}\cdot\boldsymbol{y}\}, \tag{12}$$

denoting the *far-field pattern* of $\Phi_{\mathrm{e}}(\boldsymbol{x},\boldsymbol{y})$. A direct consequence of (9) and (12) is that the scattered field u^{sct} exhibits an asymptotic behaviour of the form

$$u^{\mathrm{sct}}(\boldsymbol{x};\hat{\boldsymbol{d}})=\frac{\mathrm{e}^{\mathrm{i}k_{\mathrm{e}}|\boldsymbol{x}|}}{|\boldsymbol{x}|}u^{\infty}(\hat{\boldsymbol{x}};\hat{\boldsymbol{d}})+\mathcal{O}(|\boldsymbol{x}|^{-2}),\qquad |\boldsymbol{x}|\to\infty, \tag{13}$$

uniformly in all directions $\hat{\boldsymbol{x}}\in\Omega$ with the far-field pattern $u^{\infty}\colon\Omega\times\Omega\to\mathbb{C}$ being an analytic function of both its arguments and determined by

$$u^{\infty}(\hat{\boldsymbol{x}};\hat{\boldsymbol{d}})=\frac{1}{4\pi}\int_{\partial D}\left[u^{\mathrm{sct}}(\boldsymbol{y};\hat{\boldsymbol{d}})\frac{\partial\mathrm{e}^{-\mathrm{i}k_{\mathrm{e}}\hat{\boldsymbol{x}}\cdot\boldsymbol{y}}}{\partial\hat{\boldsymbol{\nu}}(\boldsymbol{y})}-\frac{\partial u^{\mathrm{sct}}(\boldsymbol{y};\hat{\boldsymbol{d}})}{\partial\hat{\boldsymbol{\nu}}(\boldsymbol{y})}\mathrm{e}^{-\mathrm{i}k_{\mathrm{e}}\hat{\boldsymbol{x}}\cdot\boldsymbol{y}}\right]\mathrm{d}s(\boldsymbol{y}),\qquad \hat{\boldsymbol{x}}\in\Omega. \tag{14}$$

The *inverse acoustic transmission scattering problem* we will be concerned with in the rest of this work can now be set forth as a task of reconstructing the shape of the scatterer D from the knowledge of the far-field patterns $u^{\infty}(\hat{\boldsymbol{x}};\hat{\boldsymbol{d}})$ caused by the scattering of acoustic plane waves of fixed frequency from an isotropic and homogeneous penetrable scatterer for all directions of observation $\hat{\boldsymbol{x}}\in\Omega$ and all directions of incidence $\hat{\boldsymbol{d}}\in\Omega$. For a uniqueness result concerning this inverse problem we refer the reader to [36].

Aiming at analyzing the above stated inverse scattering problem within the framework of the factorization method, one finds it extremely useful to consider the most general (regular) incidence consisting of a linear combination of plane waves with appropriate weights. This notion leads to the introduction of *acoustic Herglotz wave functions* [16]. More precisely, a Herglotz wave function v_g with kernel (or density) $g\in L^2(\Omega)$ is defined by

$$v_g(\boldsymbol{x}):=\int_{\Omega}\mathrm{e}^{\mathrm{i}k_{\mathrm{e}}\boldsymbol{x}\cdot\hat{\boldsymbol{d}}}g(\hat{\boldsymbol{d}})\,\mathrm{d}s(\hat{\boldsymbol{d}}),\qquad \boldsymbol{x}\in\mathbb{R}^3. \tag{15}$$

One may now take advantage of the well-known superposition principle [16], according to which, the far-field pattern, say $v^{\infty}(\hat{\boldsymbol{x}})$, $\hat{\boldsymbol{x}}\in\Omega$, of the scattered field $v^{\mathrm{sct}}(\boldsymbol{x})$, $\boldsymbol{x}\in\mathbb{R}^3\backslash\overline{D}$, generated by the incidence of a superposition of incident plane waves of the form (15) on the scatterer is the superposition of the far-field patterns corresponding to the scattered fields caused by the incidence of the individual plane waves. Consequently, one has that

$$v^{\infty}(\hat{\boldsymbol{x}})=\int_{\Omega}u^{\infty}(\hat{\boldsymbol{x}};\hat{\boldsymbol{d}})g(\hat{\boldsymbol{d}})\,\mathrm{d}s(\hat{\boldsymbol{d}}),\qquad \hat{\boldsymbol{x}}\in\Omega,$$

which leads in a natural way to the introduction of the *far-field operator* $F\colon L^2(\Omega) \to L^2(\Omega)$ corresponding to the scattering problem (4)–(8) through the relation $(Fg)(\hat{\boldsymbol{x}}) := v^\infty(\hat{\boldsymbol{x}})$, $\hat{\boldsymbol{x}} \in \Omega$, i.e., F is the linear integral operator

$$(Fg)(\hat{\boldsymbol{x}}) = \int_\Omega u^\infty(\hat{\boldsymbol{x}}; \hat{\boldsymbol{d}}) g(\hat{\boldsymbol{d}})\, \mathrm{d}s(\hat{\boldsymbol{d}}), \qquad \hat{\boldsymbol{x}} \in \Omega, \tag{16}$$

whose integral kernel is formed by the forward data of the inverse problem.

3. Factorization of the far-field operator for the acoustic transmission problem

We first of all note that the objective of the factorization method is to provide an explicit characterization of the shape of the unknown scattering obstacle D by the 'data operator' F. Originally proposed by Kirsch in [28] for the acoustic scattering problem by a soft or hard scatterer, the $(F^*F)^{1/4}$-variant of the specific inverse scattering technique (see [34] for a detailed description of other variants of the method) tries to overcome the difficulty of explicitly constructing elements of the range $\mathcal{R}(F)$ of F by first establishing an explicit relation between the shape of D and the range of an operator which is closely related to F, namely the linear operator $G\colon H^{1/2}(\partial D) \times H^{-1/2}(\partial D) \to L^2(\Omega)$, defined by $G(f,h) := u^\infty$, where $u^\infty \in L^2(\Omega)$ is the far-field pattern of the scattered solution of TP with boundary data $(f,h) \in H^{1/2}(\partial D) \times H^{-1/2}(\partial D)$. A second step, which actually constitutes the cornerstone for the applicability of the method, consists of an attempt to provide a precise characterization of $\mathcal{R}(G)$ by the data operator F by proving that $\mathcal{R}(G) = \mathcal{R}\big((F^*F)^{1/4}\big)$. The proof of the last assertion is the most demanding part of the method and is accomplished by establishing an appropriate operator factorization of F with the involved operators enjoying specific properties as it will be clarified shortly.

Before proceeding any further, let us comment as briefly as possible on the main properties of the far-field operator F, some of which are, in fact, a fundamental prerequisite for the applicability of the $(F^*F)^{1/4}$-method (see theorem 3.3 below). In particular, F is certainly compact on $L^2(\Omega)$ (due to the analyticity of its kernel) and enjoys a *normality* property, i.e.,

$$F^*F = FF^*, \tag{17}$$

with $F^*\colon L^2(\Omega) \to L^2(\Omega)$ denoting its adjoint with respect to the (conjugate linear in the first argument) inner product on $L^2(\Omega)$ (see definition (23) below). Moreover, the *scattering operator* $\mathcal{S}\colon L^2(\Omega) \to L^2(\Omega)$, which is connected to F through the relation $\mathcal{S} := I + \mathrm{i}\frac{k_e}{2\pi}F$, is *unitary*, that is,

$$\mathcal{S}^*\mathcal{S} = \mathcal{S}\mathcal{S}^* = I, \tag{18}$$

with I standing for the identity operator. Properties (17) and (18) can easily be proved to hold true for the far-field operator corresponding to the transmission problem (4)–(8) by following the arguments presented in [27, Chapter 5]. Another key property of F is its injectivity. A well known result (see, e.g., [16, 27]) states that F is one-to-one

if, and only if, there does not exist a Herglotz wave function v with non-trivial density $g \in L^2(\Omega)$ such that the function pair (w, v), with $w, v \in C^2(D) \cap C^1(\overline{D})$, solves the following *classical interior transmission problem*

$$\Delta w(\boldsymbol{x}) + k_{\mathrm{i}}^2 w(\boldsymbol{x}) = 0, \qquad \boldsymbol{x} \in D, \tag{19}$$

$$\Delta v(\boldsymbol{x}) + k_{\mathrm{e}}^2 v(\boldsymbol{x}) = 0, \qquad \boldsymbol{x} \in D, \tag{20}$$

$$w(\boldsymbol{x}) - v(\boldsymbol{x}) = f(\boldsymbol{x}), \qquad \boldsymbol{x} \in \partial D, \tag{21}$$

$$\tau^{-1} \frac{\partial w}{\partial \hat{\boldsymbol{\nu}}}(\boldsymbol{x}) - \frac{\partial v}{\partial \hat{\boldsymbol{\nu}}}(\boldsymbol{x}) = h(\boldsymbol{x}), \qquad \boldsymbol{x} \in \partial D, \tag{22}$$

with homogeneous boundary conditions, i.e., boundary data $f = h = 0$. Values of the angular frequency ω for which a non-trivial solution to the homogeneous interior transmission problem exists consist the eigenvalues of this unconventional BVP, which are usually referred to as *interior transmission eigenvalues*¶. The scientific interest in the investigation of the interior transmission problem (ITP) with emphasis to its spectral properties (existence and countability of eigenvalues) has significantly increased over the last few years thus leading to important advancements in this area and rendering the study of ITP one of today's research subjects in inverse scattering theory (see, e.g., [12] and references therein). In the present work, similarly to any primary study of the factorization method for an inverse scattering problem involving a penetrable scatterer, we will not evoke any arguments exploring the issue of existence of the ITP spectrum, but solely exploit its discreteness. Obviously, the injectivity of F is guaranteed under the assumption that the plane wave excitation frequency ω does not coincide with an interior transmission eigenvalue. For completeness we also recall that if the nullspace $\mathcal{N}(F)$ of F is trivial then its range is dense in $L^2(\Omega)$ due to the well-known relation $F^* g = \overline{R_r F R_r \overline{g}}$ for all $g \in L^2(\Omega)$ via the reflection operator $(R_r g)(\hat{\boldsymbol{x}}) := g(-\hat{\boldsymbol{x}})$ for $\hat{\boldsymbol{x}} \in \Omega$ with the overbar indicating complex conjugation.

We now turn our attention to the investigation of the properties of the 'data-to-pattern' operator $G\colon H^{1/2}(\partial D) \times H^{-1/2}(\partial D) \to L^2(\Omega)$, defined previously, by first noting that it is bounded due to the continuous dependence of the radiating solution u to the Helmholtz equation on the boundary data, i.e., the well-posedness of TP. Generally speaking, its range $\mathcal{R}(G)$ is 'much larger' than $\mathcal{R}(F)$. In a first step, the next theorem proves, among others, that it is dense in $L^2(\Omega)$. For later reference, let us introduce at this point some terminology. We define the product space $X := H^{1/2}(\partial D) \times H^{-1/2}(\partial D)$ and abbreviate $Y := L^2(\Omega)$. The Hilbert space Y is equipped with the inner product

$$(g_1, g_2)_Y := \int_\Omega \overline{g_1(\hat{\boldsymbol{x}})} g_2(\hat{\boldsymbol{x}}) \, \mathrm{d}s(\hat{\boldsymbol{x}}) \quad \text{for all } g_1, g_2 \in Y. \tag{23}$$

By denoting with X^* the dual space of X, we consider the usual duality pairing in

¶ We refer to k_{e} since k_{i} can obviously be written as $k_{\mathrm{i}} = k_{\mathrm{e}}\sqrt{n}$ with the index of refraction $n := c_{\mathrm{e}}^2/c_{\mathrm{i}}^2$ being a positive constant.

$\langle\cdot,\cdot\rangle_{X^*\times X}$ and the induced sesquilinear form

$$\begin{aligned}\big((h_2,f_2),(f_1,h_1)\big)_{X^*\times X} &:= \langle(\overline{h_2},\overline{f_2}),(f_1,h_1)\rangle_{X^*\times X}\\ &:= \int_{\partial D}\overline{h_2(\boldsymbol{x})}f_1(\boldsymbol{x})\,\mathrm{d}s(\boldsymbol{x}) + \int_{\partial D}\overline{f_2(\boldsymbol{x})}h_1(\boldsymbol{x})\,\mathrm{d}s(\boldsymbol{x}),\end{aligned}\tag{24}$$

for $(f_1,h_1)\in X$ and $(h_2,f_2)\in X^*$. Finally, we will make use of the notations $\langle h,f\rangle_c := \langle\overline{h},f\rangle$ for $h\in H^{-1/2}(\partial D)$, $f\in H^{1/2}(\partial D)$, with $\langle\cdot,\cdot\rangle$ denoting the usual duality pairing between $H^{-1/2}(\partial D)$ and $H^{1/2}(\partial D)$, and $\partial_{\hat{\boldsymbol{\nu}}} := \partial/\partial\hat{\boldsymbol{\nu}}$ for the normal derivative operator.

Theorem 3.1. *The range $\mathcal{R}(G)$ of the operator $G\colon X\to Y$ is dense in Y. Moreover, for the range $\mathcal{R}(G^*)$ of the adjoint operator $G^*\colon Y\to X^*$ the following characterization holds*

$$4\pi G^*g = (-\tau^{-1}\partial_{\hat{\boldsymbol{\nu}}}w_0|_{\partial D}, w_0|_{\partial D}),\tag{25}$$

where $g\in Y$ and w_0 is the complex conjugate of the function which represents the interior field of the unique function pair solving the transmission problem with the Herglotz data $(\overline{v_g}|_{\partial D},\partial_{\hat{\boldsymbol{\nu}}}\overline{v_g}|_{\partial D})$ as boundary data.

Proof. The proof is exactly analogous to the proof of [11, Theorem 4.1], where the corresponding result is established for the case of an anisotropic inhomogeneous scatterer in three dimensions, and is therefore omitted for brevity. □

It is worthwhile noticing that, in contrast to the impenetrable scatterer case (i.e., acoustically soft or hard scatterer), the operator G corresponding to the transmission problem fails to be injective. This claim can be confirmed by employing the space relation (see, e.g., [49])

$$\begin{aligned}\mathcal{N}(G) &= {}^{\alpha}[\mathcal{R}(G^*)]\\ &:= \Big\{(f_N,h_N)\in X : \big((h',f'),(f_N,h_N)\big)_{X^*\times X} = 0 \quad \text{for all } (h',f')\in\mathcal{R}(G^*)\Big\},\end{aligned}\tag{26}$$

which in combination with the characterization (25) of G^* and the definition (24), implies that if $(f_N,h_N)\in\mathcal{N}(G)$ then

$$\int_{\partial D}\Big\{\big[-\tau^{-1}\overline{\partial_{\hat{\boldsymbol{\nu}}}w_0}\big]f_N + \overline{w_0}\,h_N\Big\}\mathrm{d}s = 0,\tag{27}$$

for every $\overline{w_0}$ which is the interior field of the solution to the transmission scattering problem with Herglotz boundary data $(\overline{v_g}|_{\partial D},\partial_{\hat{\boldsymbol{\nu}}}\overline{v_g}|_{\partial D})$ for some $g\in Y$. The question arising is whether non-trivial pairs (f_N,h_N) satisfying (27) exist. This question is answered affirmatively, since by considering any solution $w\in H^1(D)$ of the Helmholtz equation (4) in D, the pair $(f_N,h_N) := (w|_{\partial D},\tau^{-1}\partial_{\hat{\boldsymbol{\nu}}}w|_{\partial D})$ belongs to X and satisfies (27) as one may confirm by applying Green's second integral theorem to the functions w and $\overline{w_0}$ in D. Consequently, the operator G annihilates every element of X which constitutes pair of interior traces (trace and, up to a multiplicative factor, normal derivative) on the boundary ∂D of solutions to the interior Helmholtz equation in D. This property will be utilized in the proof of the following theorem, in which the ability of constructing explicit elements of $\mathcal{R}(G)$ is impressed.

Theorem 3.2. *For any $\boldsymbol{z} \in \mathbb{R}^3$, $\Phi_{\mathrm{e}}^{\infty}(\cdot, \boldsymbol{z}) \in \mathcal{R}(G)$ if, and only if, $\boldsymbol{z} \in D$.*

Proof. For $\boldsymbol{z} \in D$, define $v(\boldsymbol{x}) := \Phi_{\mathrm{e}}(\boldsymbol{x}, \boldsymbol{z})$, $\boldsymbol{x} \in \mathbb{R}^3 \backslash \overline{D}$, which is a radiating solution of Helmholtz equation outside D with far-field pattern $v^{\infty}(\hat{\boldsymbol{x}}) = \Phi_{\mathrm{e}}^{\infty}(\hat{\boldsymbol{x}}, \boldsymbol{z})$, $\hat{\boldsymbol{x}} \in \Omega$. Denoting by γ the trace operator and employing the superscripts $(+)$ and $(-)$ to denote the limit obtained by approaching ∂D from $\mathbb{R}^3 \backslash \overline{D}$ and D, respectively, we have that $\gamma^{+} v \in H^{1/2}(\partial D)$ and $\partial_{\boldsymbol{\nu}}^{+} v \in H^{-1/2}(\partial D)$ since $v \in H_{\mathrm{loc}}^{1}(\mathbb{R}^3 \backslash \overline{D})$ and, clearly, Δv is square-integrable in a neighborhood of ∂D. We now consider an arbitrary function $w \in H^1(D)$ solving Helmholtz equation (with wavenumber k_{i}) in D. Clearly, $\gamma^{-} w \in H^{1/2}(\partial D)$ and $\partial_{\boldsymbol{\nu}}^{-} w \in H^{-1/2}(\partial D)$ and we can then define $f := \gamma^{-} w - \gamma^{+} v \in H^{1/2}(\partial D)$ and $h := \tau^{-1} \partial_{\boldsymbol{\nu}}^{-} w - \partial_{\boldsymbol{\nu}}^{+} v \in H^{-1/2}(\partial D)$. Thus, by construction, the pair $(w, v) \in H^1(D) \times H_{\mathrm{loc}}^{1}(\mathbb{R}^3 \backslash \overline{D})$ satisfies the differential equations of TP as well as the boundary conditions with data $(f, h) \in X$. Hence, by definition of G, there holds that $G(f, h) = v^{\infty}$, whence $\Phi_{\mathrm{e}}^{\infty}(\cdot, \boldsymbol{z}) \in \mathcal{R}(G)$ follows. (One may note that the arbitrariness in the choice of the interior field is nonessential since the pair of its traces will be annihilated by G in any case, i.e., one can also write $G(\Phi_{\mathrm{e}}(\cdot, \boldsymbol{z})|_{\partial D}, \partial_{\boldsymbol{\nu}} \Phi_{\mathrm{e}}(\cdot, \boldsymbol{z})|_{\partial D}) = -\Phi_{\mathrm{e}}^{\infty}(\cdot, \boldsymbol{z})$.)

Let now $\boldsymbol{z} \notin D$ and assume on the contrary that there exist some $(f, h) \in X$ such that $G(f, h) = \Phi_{\mathrm{e}}^{\infty}(\cdot, \boldsymbol{z})$. Let then (w, v) denote the solution pair of TP with boundary data (f, h). Then $v^{\infty} = G(f, h)$ follows by the definition of G. Since $\Phi_{\mathrm{e}}^{\infty}(\cdot, \boldsymbol{z})$ is the far-field pattern of the radiating field $\Phi_{\mathrm{e}}(\cdot, \boldsymbol{z})$, Rellich's lemma assures us that $v(\boldsymbol{x}) = \Phi_{\mathrm{e}}(\boldsymbol{x}, \boldsymbol{z})$ for every $\boldsymbol{x}$ lying in the exterior of any sphere containing both $\overline{D}$ and $\boldsymbol{z}$. If $\boldsymbol{z} \notin \overline{D}$, we have a contradiction due to the fact that the radiating part v of the solution pair (w, v) is an analytic function in $\mathbb{R}^3 \backslash \overline{D}$ while $\Phi_{\mathrm{e}}(\boldsymbol{x}, \boldsymbol{z})$ has a singularity at $\boldsymbol{x} = \boldsymbol{z}$. If $\boldsymbol{z} \in \partial D$, from the boundary conditions of TP we see that the restrictions of $\Phi_{\mathrm{e}}(\cdot, \boldsymbol{z})$ on ∂D are $\Phi_{\mathrm{e}}(\cdot, \boldsymbol{z})|_{\partial D} \in H^{1/2}(\partial D)$ and $\partial_{\hat{\boldsymbol{\nu}}} \Phi_{\mathrm{e}}(\cdot, \boldsymbol{z})|_{\partial D} \in H^{-1/2}(\partial D)$. But this certainly contradicts the fact that (the radiating solution of Helmholtz equation) $\Phi_{\mathrm{e}}(\boldsymbol{x}, \boldsymbol{z})$ for $\boldsymbol{x} \to \boldsymbol{z} \in \partial D$ exhibits the singular behaviour

$$\Phi_{\mathrm{e}}(\boldsymbol{x}, \boldsymbol{z}) = \mathcal{O}\left(\frac{1}{|\boldsymbol{x} - \boldsymbol{z}|}\right), \qquad \boldsymbol{\nabla} \Phi_{\mathrm{e}}(\boldsymbol{x}, \boldsymbol{z}) = \mathcal{O}\left(\frac{1}{|\boldsymbol{x} - \boldsymbol{z}|^2}\right), \qquad |\boldsymbol{x} - \boldsymbol{z}| \to 0, \tag{28}$$

which, in particular, implies that $\Phi_{\mathrm{e}}(\cdot, \boldsymbol{z}) \notin H_{\mathrm{loc}}^{1}(\mathbb{R}^3 \backslash \overline{D})$. □

We proceed further by remarking that in the present study the derivation of the crucial equality $\mathcal{R}(G) = \mathcal{R}\big((F^{*} F)^{1/4}\big)$ will be based on the application of the following abstract result from functional analysis, which is proved in the monograph [34] by Kirsch and Grinberg (see also [17]), to the far-field operator F.

Theorem 3.3. *Let U be a Hilbert space, Z a reflexive Banach space and let the compact operator $F \colon U \to U$ have a factorization of the form*

$$F = \mathcal{D} \mathcal{T} \mathcal{D}^{*}, \tag{29}$$

with bounded linear operators $\mathcal{D} \colon Z \to U$ and $\mathcal{T} \colon Z^{*} \to Z$. Assume that:
(a) $\operatorname{Im} \langle \phi, \mathcal{T} \phi \rangle_{Z^{*} \times Z} \neq 0$ *for all* $\phi \in \overline{\mathcal{R}(\mathcal{D}^{*})}$ *with* $\phi \neq 0$*;*

(b) $\mathcal{T}$ is of the form $\mathcal{T} = \mathcal{T}_0 + \mathcal{L}$ for some compact operator $\mathcal{L}$ and some self-adjoint operator $\mathcal{T}_0$, which is strictly coercive on $\mathcal{R}(\mathcal{D}^*)$, i.e., there exists $c > 0$ such that

$$\big|\langle \phi, \mathcal{T}_0 \phi \rangle_{Z^* \times Z}\big| \geqslant c \|\phi\|^2_{Z^*} \quad \text{for all } \phi \in \mathcal{R}(\mathcal{D}^*); \tag{30}$$

(c) F is injective and $I_U + \mathrm{i}\gamma F$ is unitary for some $\gamma > 0$.

Then the ranges of $\mathcal{D}$ and $(F^*F)^{1/4}$ coincide. If, in addition, the operator $\mathcal{D}$ is one-to-one then $(F^*F)^{-1/4}\mathcal{D}$ and $\mathcal{D}^{-1}(F^*F)^{1/4}$ are continuous isomorphisms from Z onto U and from U onto Z, respectively.

By identifying, here and in the following, U with $Y = L^2(\Omega)$ and recalling our discussion on the properties of F, assumption (c) is clearly satisfied. We would like to note in advance that the forthcoming analysis, which aims at deriving a factorization of F of the form (29) with the participating operators meeting assumptions (a) and (b), mobilizes some of the arguments presented by the authors in reference [13], wherein the inverse transmission scattering problem in elasticity is investigated within the framework of the factorization method. Both for the sake of brevity and to avoid 'repetitions', we have preferred to refer the reader to this study for the proof details of some results, whenever these proofs are recoverable by a simple reduction from the elastic to the acoustic case, with the hope that this strategy is not at the expense of the present work's clarity.

As one might expect, the starting point for establishing a factorization of F of the form (29) is its representation as $F = GH$ in terms of G and an auxiliary operator $H\colon Y \to X$ mapping the density $g \in Y$ of the Herglotz wave function v_g to the pair consisting of the trace and the normal derivative of v_g on the boundary and thus defined by

$$\begin{aligned}(Hg)(\boldsymbol{x}) &:= \big(v_g(\boldsymbol{x}),\, \partial_{\hat{\boldsymbol{\nu}}(\boldsymbol{x})} v_g(\boldsymbol{x})\big), \qquad \boldsymbol{x} \in \partial D,\\ &= \left(\int_\Omega \mathrm{e}^{\mathrm{i}k_\mathrm{e}\boldsymbol{x}\cdot\hat{\boldsymbol{d}}} g(\hat{\boldsymbol{d}})\, \mathrm{d}s(\hat{\boldsymbol{d}}),\, \int_\Omega \frac{\partial \mathrm{e}^{\mathrm{i}k_\mathrm{e}\boldsymbol{x}\cdot\hat{\boldsymbol{d}}}}{\partial \hat{\boldsymbol{\nu}}(\boldsymbol{x})} g(\hat{\boldsymbol{d}})\, \mathrm{d}s(\hat{\boldsymbol{d}}) \right), \qquad \boldsymbol{x} \in \partial D,\end{aligned} \tag{31}$$

and referred to as the *Herglotz operator*. As a next step, one tries to characterize the Herglotz operator H via the operator G itself. To this end, we construct the adjoint operator $H^*\colon X^* \to Y$ as follows: an element $g^* \in Y$ is equal to the image of an element $(h, f) \in X^*$ under the action of the operator H^* if, and only if,

$$\big((h, f), Hg\big)_{X^* \times X} = (g^*, g)_Y \quad \text{for all } g \in Y. \tag{32}$$

With the aid of the definitions (23), (24), and (31) and after interchanging the order of integration in the left-hand side of (32), one easily finds that

$$\big(H^*(h, f)\big)(\hat{\boldsymbol{x}}) = \int_{\partial D} \mathrm{e}^{-\mathrm{i}k_\mathrm{e}\hat{\boldsymbol{x}}\cdot\boldsymbol{y}} h(\boldsymbol{y})\, \mathrm{d}s(\boldsymbol{y}) + \int_{\partial D} \frac{\partial \mathrm{e}^{-\mathrm{i}k_\mathrm{e}\hat{\boldsymbol{x}}\cdot\boldsymbol{y}}}{\partial \hat{\boldsymbol{\nu}}(\boldsymbol{y})} f(\boldsymbol{y})\, \mathrm{d}s(\boldsymbol{y}), \qquad \hat{\boldsymbol{x}} \in \Omega. \tag{33}$$

By virtue of the asymptotic behaviour of the fundamental solution Φ_e (see (11), (12)), one then concludes that $H^*(h, f)$ is, up to a factor 4π, the far-field pattern $v^\infty(\hat{\boldsymbol{x}})$, $\hat{\boldsymbol{x}} \in \Omega$ of the combined field

$$v(\boldsymbol{x}) := \mathrm{SL}_\mathrm{e} h(\boldsymbol{x}) + \mathrm{DL}_\mathrm{e} f(\boldsymbol{x}), \qquad \boldsymbol{x} \in \mathbb{R}^3 \backslash \overline{D}, \tag{34}$$

in terms of the acoustic single- and double-layer potentials defined by

$$\mathrm{SL}_a\psi(\boldsymbol{x}) = \int_{\partial D} \Phi_a(\boldsymbol{x},\boldsymbol{y})\,\psi(\boldsymbol{y})\,\mathrm{d}s(\boldsymbol{y}), \qquad \boldsymbol{x}\notin\partial D, \tag{35}$$

and

$$\mathrm{DL}_a\phi(\boldsymbol{x}) = \int_{\partial D} \frac{\partial\Phi_a(\boldsymbol{x},\boldsymbol{y})}{\partial\hat{\boldsymbol{\nu}}(\boldsymbol{y})}\,\phi(\boldsymbol{y})\,\mathrm{d}s(\boldsymbol{y}), \qquad \boldsymbol{x}\notin\partial D, \tag{36}$$

respectively, with $a = \{\mathrm{e},\mathrm{i}\}$, depending on the physical parameters involved and densities $\psi \in H^{-1/2}(\partial D)$ and $\phi \in H^{1/2}(\partial D)$. Thus, we have shown that $\big(H^*(h,f)\big)(\hat{\boldsymbol{x}}) = 4\pi v^\infty(\hat{\boldsymbol{x}})$, $\hat{\boldsymbol{x}}\in\Omega$. On the other hand, the radiating field $v(\boldsymbol{x})$, $\boldsymbol{x}\in\mathbb{R}^3\backslash\overline{D}$ can be seen as the radiating part (i.e., the scattered field) of the solution to TP corresponding to some surface data. Its trace and normal derivative on the scatterer's surface are determined via jump relations of the involved layer potentials. In particular, we obtain that

$$\begin{aligned}\gamma^+ v(\boldsymbol{x}) &= \gamma^+(\mathrm{SL_e}h)(\boldsymbol{x}) + \gamma^+(\mathrm{DL_e}f)(\boldsymbol{x})\\ &= (S_\mathrm{e}h)(\boldsymbol{x}) + \frac{1}{2}\big[f(\boldsymbol{x}) + (K_\mathrm{e}f)(\boldsymbol{x})\big], \qquad \boldsymbol{x}\in\partial D,\end{aligned} \tag{37}$$

$$\begin{aligned}\partial^+_{\hat{\boldsymbol{\nu}}(\boldsymbol{x})} v(\boldsymbol{x}) &= \partial^+_{\hat{\boldsymbol{\nu}}(\boldsymbol{x})}(\mathrm{SL_e}h)(\boldsymbol{x}) + \partial^+_{\hat{\boldsymbol{\nu}}(\boldsymbol{x})}(\mathrm{DL_e}f)(\boldsymbol{x})\\ &= \frac{1}{2}\big[-h(\boldsymbol{x}) + (K'_\mathrm{e}h)(\boldsymbol{x})\big] - (R_\mathrm{e}f)(\boldsymbol{x}), \qquad \boldsymbol{x}\in\partial D,\end{aligned} \tag{38}$$

where the boundary integral operators S_a, K_a, K'_a, R_a, $a = \{\mathrm{e},\mathrm{i}\}$, are defined as follows[+] [49]

$$(S_a\psi)(\boldsymbol{x}) = \int_{\partial D} \Phi_a(\boldsymbol{x},\boldsymbol{y})\,\psi(\boldsymbol{y})\,\mathrm{d}s(\boldsymbol{y}), \qquad \boldsymbol{x}\in\partial D, \tag{39}$$

$$(K_a\psi)(\boldsymbol{x}) = 2\int_{\partial D} \frac{\partial\Phi_a(\boldsymbol{x},\boldsymbol{y})}{\partial\hat{\boldsymbol{\nu}}(\boldsymbol{y})}\,\psi(\boldsymbol{y})\,\mathrm{d}s(\boldsymbol{y}), \qquad \boldsymbol{x}\in\partial D, \tag{40}$$

$$(K'_a\psi)(\boldsymbol{x}) = 2\int_{\partial D} \frac{\partial\Phi_a(\boldsymbol{x},\boldsymbol{y})}{\partial\hat{\boldsymbol{\nu}}(\boldsymbol{x})}\,\psi(\boldsymbol{y})\,\mathrm{d}s(\boldsymbol{y}), \qquad \boldsymbol{x}\in\partial D, \tag{41}$$

$$(R_a\phi)(\boldsymbol{x}) = -\frac{\partial}{\partial\hat{\boldsymbol{\nu}}(\boldsymbol{x})}\int_{\partial D} \frac{\partial\Phi_a(\boldsymbol{x},\boldsymbol{y})}{\partial\hat{\boldsymbol{\nu}}(\boldsymbol{y})}\,\phi(\boldsymbol{y})\,\mathrm{d}s(\boldsymbol{y}), \qquad \boldsymbol{x}\in\partial D, \tag{42}$$

for densities $\psi\in H^{-1/2}(\partial D)$ and $\phi\in H^{1/2}(\partial D)$. For an intensive study of the mapping properties of these operators in Sobolev spaces we refer again to [49]. In our context we simply recall that the operators S_a, K_a, K'_a are bounded from $H^{-1/2}(\partial D)$ into $H^{1/2}(\partial D)$ and the operator R_a is bounded from $H^{1/2}(\partial D)$ into $H^{-1/2}(\partial D)$ (see, e.g., [26]). We denote by $\overline{\mathrm{SL}_a}\psi$ and $\overline{\mathrm{DL}_a}\phi$ the layer potentials with kernels based on the complex-conjugate of the fundamental solution, i.e., Φ_a is replaced by $\overline{\Phi_a}$ in definitions (35) and (36). This gives rise to the adjoints (with respect to the sesquilinear form $\langle\cdot,\cdot\rangle_c$ defined previously) of the above surface integral operators; namely[*]

$$(S_a^*\psi)(\boldsymbol{x}) = \int_{\partial D} \overline{\Phi_a(\boldsymbol{x},\boldsymbol{y})}\,\psi(\boldsymbol{y})\,\mathrm{d}s(\boldsymbol{y}), \qquad \boldsymbol{x}\in\partial D, \tag{43}$$

[+] Note that the operator K'_a is the transpose of K_a.

[*] It is noted that $(K'_a)^* = \overline{(K'_a)'} = \overline{K_a}$ and $K_a^* = \overline{K_a}' = \overline{K_a}'$.

$$(\overline{K_a}\psi)(\boldsymbol{x}) = 2\int_{\partial D} \frac{\partial\overline{\Phi_a(\boldsymbol{x},\boldsymbol{y})}}{\partial\hat{\boldsymbol{\nu}}(\boldsymbol{y})}\,\psi(\boldsymbol{y})\,\mathrm{d}s(\boldsymbol{y}), \qquad \boldsymbol{x}\in\partial D, \tag{44}$$

$$(K_a^*\psi)(\boldsymbol{x}) = 2\int_{\partial D} \frac{\partial\overline{\Phi_a(\boldsymbol{x},\boldsymbol{y})}}{\partial\hat{\boldsymbol{\nu}}(\boldsymbol{x})}\,\psi(\boldsymbol{y})\,\mathrm{d}s(\boldsymbol{y}), \qquad \boldsymbol{x}\in\partial D, \tag{45}$$

$$(R_a^*\phi)(\boldsymbol{x}) = -\frac{\partial}{\partial\hat{\boldsymbol{\nu}}(\boldsymbol{x})}\int_{\partial D} \frac{\partial\overline{\Phi_a(\boldsymbol{x},\boldsymbol{y})}}{\partial\hat{\boldsymbol{\nu}}(\boldsymbol{y})}\,\phi(\boldsymbol{y})\,\mathrm{d}s(\boldsymbol{y}), \qquad \boldsymbol{x}\in\partial D, \tag{46}$$

which share similar functional theoretic properties.

We may now return to relations (37) and (38) representing the trace and the normal derivative of the scattered field $v(\boldsymbol{x})$, $\boldsymbol{x}\in\mathbb{R}^3\backslash\overline{D}$ and its connection to the operator H^* through (34) and note that the boundary data of the corresponding TP whose unique solution pair has a radiating part which coincides with $\boldsymbol{v}$ in $\mathbb{R}^3\backslash\overline{D}$ will, of course, be the pair $(-\gamma^+v(\boldsymbol{x})+\gamma^-v^{\mathrm{i}}(\boldsymbol{x}), -\partial^+_{\hat{\boldsymbol{\nu}}(\boldsymbol{x})}v(\boldsymbol{x})+\tau^{-1}\partial^-_{\hat{\boldsymbol{\nu}}(\boldsymbol{x})}v^{\mathrm{i}}(\boldsymbol{x}))$, $\boldsymbol{x}\in\partial D$ with v^{i} denoting the accompanying transmitted field. Consequently, (34) now reads

$$4\pi G(-\gamma^+v+\gamma^-v^{\mathrm{i}}, -\partial^+_{\hat{\boldsymbol{\nu}}}v+\tau^{-1}\partial^-_{\hat{\boldsymbol{\nu}}}v^{\mathrm{i}}) = H^*(h,f). \tag{47}$$

Given that $(\gamma^-v^{\mathrm{i}}, \tau^{-1}\partial^-_{\hat{\boldsymbol{\nu}}}v^{\mathrm{i}})\in\mathcal{N}(G)$, as it has already been shown, we clearly have that

$$H^*(h,f) = -4\pi G(\gamma^+v, \partial^+_{\hat{\boldsymbol{\nu}}}v), \tag{48}$$

and by taking into account (37) and (38) we deduce that $H^* = -4\pi GB$, where B is the matrix integral operator

$$B := \begin{bmatrix} S_{\mathrm{e}} & \frac{1}{2}(I+K_{\mathrm{e}}) \\ \frac{1}{2}(-I+K'_{\mathrm{e}}) & -R_{\mathrm{e}} \end{bmatrix}. \tag{49}$$

As a result, $H = -4\pi B^*G^*$ which, when combined with the fundamental representation $F = GH$, leads to the following decomposition of the far-field operator

$$F = -4\pi GB^*G^*. \tag{50}$$

However, the operator G fails to be injective and the adjoint of B is far from meeting the assumptions concerning the operator $\mathcal{T}$ appeared in (29).

Our plan of overcoming these difficulties includes, as a first step, a deeper investigation of the operator G. We define the *Steklov-Poincaré operator* Λ_{i}, which maps continuously $H^{1/2}(\partial D)$ onto $H^{-1/2}(\partial D)$ in case that k_{i}^2 is neither a Dirichlet eigenvalue nor a Neumann eigenvalue of $-\Delta$ in D. This is actually the Dirichlet-to-Neumann map assigning to the Dirichlet data of an interior Helmholtz equation solution its normal derivative on the boundary ∂D and possesses a continuous inverse operator. With the aid of Λ_{i}, our hitherto knowledge on the nullspace of G can be incorporated in the relation $\left\{(f,\tau^{-1}\Lambda_{\mathrm{i}}f)\colon f\in H^{1/2}(\partial D)\right\}\subset\mathcal{N}(G)$. By arguing as in reference [13], one can also establish the reverse inclusion and thus obtain the result of the next lemma.

Lemma 3.4. *Assume that k_{i}^2 is neither a Dirichlet nor a Neumann eigenvalue of $-\Delta$ in D. Then the nullspace $\mathcal{N}(G)$ of the operator G is given by the set*

$$\mathcal{N}(G) = \left\{(f,\tau^{-1}\Lambda_{\mathrm{i}}f)\,:\, f\in H^{1/2}(\partial D)\right\}. \tag{51}$$

One may now take advantage of this result to decompose the operator G appropriately in order to retain only its injective part. More precisely, we write

$$\begin{aligned} G &= G\begin{bmatrix} I & 0 \\ 0 & I \end{bmatrix} = \frac{1}{2}G\begin{bmatrix} I & \tau\Lambda_{\mathrm{i}}^{-1} \\ \tau^{-1}\Lambda_{\mathrm{i}} & I \end{bmatrix} + \frac{1}{2}G\begin{bmatrix} I & -\tau\Lambda_{\mathrm{i}}^{-1} \\ -\tau^{-1}\Lambda_{\mathrm{i}} & I \end{bmatrix} \\ &= \frac{1}{2}G\begin{pmatrix} I \\ \tau^{-1}\Lambda_{\mathrm{i}} \end{pmatrix}\begin{pmatrix} I & \tau\Lambda_{\mathrm{i}}^{-1} \end{pmatrix} + \frac{1}{2}G\begin{pmatrix} I \\ -\tau^{-1}\Lambda_{\mathrm{i}} \end{pmatrix}\begin{pmatrix} I & -\tau\Lambda_{\mathrm{i}}^{-1} \end{pmatrix} \\ &:= G_1\begin{pmatrix} I & -\tau\Lambda_{\mathrm{i}}^{-1} \end{pmatrix}, \end{aligned} \tag{52}$$

where $G_1\colon H^{1/2}(\partial D) \to Y$ is the operator defined by

$$G_1 := \frac{1}{2}G\begin{pmatrix} I \\ -\tau^{-1}\Lambda_{\mathrm{i}} \end{pmatrix}, \tag{53}$$

and we have used the annihilating property of G when acts on the range of the operator $(I, \tau^{-1}\Lambda_{\mathrm{i}})\colon H^{1/2}(\partial D) \to X$. The operator G_1 inherits the good properties of G, that is, it has dense range in Y, since G does (by theorem 3.1) and $\mathcal{R}(G) = \mathcal{R}(G_1)$ (by (52) and (53)), and simultaneously avoids the non-injectivity of G as one can easily confirm by an elementary argument using the result of lemma 3.4. Substituting the expressions of the operators B and G from equations (49) and (52), respectively, into the decomposition (50), we obtain

$$F = -4\pi G_1\begin{pmatrix} I & -\tau\Lambda_{\mathrm{i}}^{-1} \end{pmatrix}\begin{bmatrix} S_{\mathrm{e}}^* & \frac{1}{2}(-I + \overline{K_{\mathrm{e}}}) \\ \frac{1}{2}(I + K_{\mathrm{e}}^*) & -R_{\mathrm{e}}^* \end{bmatrix}\begin{pmatrix} I \\ -\tau\Lambda_{\mathrm{i}}^{-1} \end{pmatrix} G_1^*, \tag{54}$$

or, equivalently,

$$F = -4\pi G_1 B_1^* G_1^*, \tag{55}$$

where B_1^* is the adjoint of the operator B_1, with the latter defined by

$$B_1 = S_{\mathrm{e}} - \frac{\tau}{2}\Lambda_{\mathrm{i}}^{-1}K_{\mathrm{e}}' - \frac{\tau}{2}K_{\mathrm{e}}\Lambda_{\mathrm{i}}^{-1} - \tau^2\Lambda_{\mathrm{i}}^{-1}R_{\mathrm{e}}\Lambda_{\mathrm{i}}^{-1}. \tag{56}$$

It is noted that the derivation process of (55) has made use of the fact that Λ_{i} is self-adjoint, i.e., $\Lambda_{\mathrm{i}} = \Lambda_{\mathrm{i}}^*$ in the sense that $\langle \Lambda_{\mathrm{i}} f, g\rangle_c = \langle f, \Lambda_{\mathrm{i}} g\rangle_c$ for all $f, g \in H^{1/2}(\partial D)$ as one can immediately verify by an application of Green's second integral theorem. Alternatively, one can also establish the following factorization of F, which is the crucial one for our purposes, namely

$$F = -4\pi G_2 A^* G_2^*, \tag{57}$$

where the operator $G_2\colon H^{-1/2}(\partial D) \to Y$ is defined by

$$G_2 := G_1\Lambda_{\mathrm{i}}^{-1}, \tag{58}$$

and the operator $A\colon H^{1/2}(\partial D) \to H^{-1/2}(\partial D)$ is given by

$$A := \Lambda_{\mathrm{i}} S_{\mathrm{e}}\Lambda_{\mathrm{i}} - \frac{\tau}{2}K_{\mathrm{e}}'\Lambda_{\mathrm{i}} - \frac{\tau}{2}\Lambda_{\mathrm{i}}K_{\mathrm{e}} - \tau^2 R_{\mathrm{e}}. \tag{59}$$

In light of the functional analytic theorem 3.3, we identify $Z := H^{-1/2}(\partial D)$ (and hence $Z^* = H^{1/2}(\partial D)$), $\mathcal{D} := G_2$ and $\mathcal{T} := -4\pi A^*$. Clearly, the operator G_2 enjoys the

'desired' properties of G_1 since Λ_i is an isomorphism, i.e., $\mathcal{N}(G_2) = \{0\}$ and $\overline{\mathcal{R}(G_2)} = Y$ because $\mathcal{R}(G_2) = \mathcal{R}(G_1)$. What remains is to verify that the bounded operator $\mathcal{T} = -4\pi A^*$ meets the requirements (a) and (b) of theorem 3.3. In particular, the former assumption can be seen as an immediate consequence of the next lemma.

Lemma 3.5. *Assume that ω is not an interior transmission eigenvalue. Then the relation $\mathrm{Im}\langle A\phi, \phi\rangle_c = 0$ for some $\phi \in H^{1/2}(\partial D)$ implies that $\phi = 0$.*

Proof. The assertion of the lemma can be proved by arguing as in the proof of [13, Lemma 3.7], where the analogous result is established for the corresponding operator emerging during the study of the inverse elastic transmission scattering problem within the framework of the factorization method. □

Focusing now on requirement (b), we first note that $A = A_1 + L_1$, where the operator $L_1 := -\tau/2\big(K_\mathrm{e}'\Lambda_\mathrm{i} + \Lambda_\mathrm{i}K_\mathrm{e}\big)$ is compact from $H^{1/2}(\partial D)$ into $H^{-1/2}(\partial D)$ since $K_\mathrm{e}\colon H^{1/2}(\partial D) \to H^{1/2}(\partial D)$ and $K_\mathrm{e}'\colon H^{-1/2}(\partial D) \to H^{-1/2}(\partial D)$ are compact, and $A_1 := \Lambda_\mathrm{i}S_\mathrm{e}\Lambda_\mathrm{i} - \tau^2 R_\mathrm{e}$. We subsequently define the continuous operators

$$\widehat{S}_\mathrm{i} := \frac{1}{2}\big(S_\mathrm{i} + S_\mathrm{i}^*\big)\colon H^{-1/2}(\partial D) \to H^{1/2}(\partial D), \tag{60a}$$

and

$$\widehat{R}_\mathrm{i} := \frac{1}{2}\big(R_\mathrm{i} + R_\mathrm{i}^*\big)\colon H^{1/2}(\partial D) \to H^{-1/2}(\partial D), \tag{60b}$$

and rewrite A_1 as follows

$$A_1 = \underbrace{\Lambda_\mathrm{i}\widehat{S}_\mathrm{i}\Lambda_\mathrm{i} - \tau^2\widehat{R}_\mathrm{i}}_{:=A_2} + \underbrace{\Lambda_\mathrm{i}(S_\mathrm{e} - \widehat{S}_\mathrm{i})\Lambda_\mathrm{i} - \tau^2(R_\mathrm{e} - \widehat{R}_\mathrm{i})}_{:=L_2}. \tag{61}$$

The operator $S_\mathrm{e} - \widehat{S}_\mathrm{i}$ has a smooth and the operator $R_\mathrm{e} - \widehat{R}_\mathrm{i}$ has a weakly singular kernel, respectively, as one may deduce by performing a direct computation. Thus, $S_\mathrm{e} - \widehat{S}_\mathrm{i}\colon H^{-1/2}(\partial D) \to H^{1/2}(\partial D)$ and $R_\mathrm{e} - \widehat{R}_\mathrm{i}\colon H^{1/2}(\partial D) \to H^{-1/2}(\partial D)$ are compact which implies the compactness of L_2 from $H^{1/2}(\partial D)$ into $H^{-1/2}(\partial D)$. As far as the operator A_2 is concerned, one may use the properties

$$\widehat{S}_\mathrm{i} = \frac{1}{2}\Lambda_\mathrm{i}^{-1}\left[I + \frac{1}{2}\Big(K_\mathrm{i}' + K_\mathrm{i}^*\Big)\right] \qquad \text{and} \qquad \widehat{R}_\mathrm{i} = \frac{1}{2}\left[I - \frac{1}{2}\Big(K_\mathrm{i}' + K_\mathrm{i}^*\Big)\right]\Lambda_\mathrm{i},$$

to obtain that

$$\begin{aligned} A_2 &:= \Lambda_\mathrm{i}\widehat{S}_\mathrm{i}\Lambda_\mathrm{i} - \tau^2\widehat{R}_\mathrm{i} = \Lambda_\mathrm{i}\frac{1}{2}\Lambda_\mathrm{i}^{-1}\left[I + \frac{1}{2}\Big(K_\mathrm{i}' + K_\mathrm{i}^*\Big)\right]\Lambda_\mathrm{i} - \tau^2\widehat{R}_\mathrm{i} \\ &= \frac{1}{2}\left[I + \frac{1}{2}\Big(K_\mathrm{i}' + K_\mathrm{i}^*\Big)\right]\Lambda_\mathrm{i} - \tau^2\widehat{R}_\mathrm{i} \\ &= \frac{1}{2}\left[I - \frac{1}{2}\Big(K_\mathrm{i}' + K_\mathrm{i}^*\Big)\right]\Lambda_\mathrm{i} + \frac{1}{2}\Big(K_\mathrm{i}' + K_\mathrm{i}^*\Big)\Lambda_\mathrm{i} - \tau^2\widehat{R}_\mathrm{i} \\ &= \widehat{R}_\mathrm{i} + \frac{1}{2}\Big(K_\mathrm{i}' + K_\mathrm{i}^*\Big)\Lambda_\mathrm{i} - \tau^2\widehat{R}_\mathrm{i} = (1-\tau^2)\widehat{R}_\mathrm{i} + \underbrace{\frac{1}{2}\Big(K_\mathrm{i}' + K_\mathrm{i}^*\Big)\Lambda_\mathrm{i}}_{:=L_3}, \end{aligned} \tag{62}$$

with the operator $L_3\colon H^{1/2}(\partial D) \to H^{-1/2}(\partial D)$ being compact due to the compactness of K_{i}' and K_{i}^* from $H^{-1/2}(\partial D)$ into itself. By collecting all the terms we deduce that

$$A = A_0 + L_0 \quad \text{with} \quad A_0 := (1-\tau^2)\widehat{R}_{\mathrm{i}} \quad \text{and} \quad L_0 := \sum_{j=1}^{3} L_j \quad \text{compact.} \tag{63}$$

In a final step, let $R_{(k_a=\mathrm{i})}$ be the boundary operator (42) corresponding to the wavenumber $k_a = \mathrm{i}$. We abbreviate $\widetilde{R} := R_{(k_a=\mathrm{i})}$ and recall that: (i) this operator is self-adjoint and strictly coercive as an operator from $H^{1/2}(\partial D)$ onto $H^{-1/2}(\partial D)$, i.e., there exists $c_0 > 0$ such that $\langle \widetilde{R}\phi, \phi\rangle_c \geqslant c_0 \|\phi\|^2_{H^{1/2}(\partial D)}$ for all $\phi \in H^{1/2}(\partial D)$, and (ii) the difference $R_{\mathrm{i}} - \widetilde{R}\colon H^{1/2}(\partial D) \to H^{-1/2}(\partial D)$ is compact (cf., e.g., [28]). Thus, by virtue of the definition (60*b*), the operator A can be rewritten as $A = (1-\tau^2)\widetilde{R} + L_c$ for a compact operator $L_c\colon H^{1/2}(\partial D) \to H^{-1/2}(\partial D)$. Consequently, we have shown that $\mathcal{T} = \mathcal{T}_0 + \mathcal{L}$ with $\mathcal{T}_0 := -4\pi(1-\tau^2)\widetilde{R}$ and $\mathcal{L} := -4\pi L_c^*$, whence the strict coercivity (30) of $\mathcal{T}_0$ follows by that of $\widetilde{R}$, which in turn yields the applicability of theorem 3.3.

Remark 3.6. Clearly, the operator $\mathcal{T}_0$ is a continuous bijection from $H^{1/2}(\partial D)$ onto $H^{-1/2}(\partial D)$ since $\widetilde{R}$ has this property. Thus, the operator $\mathcal{T}$ differs from an isomorphism by the compact operator $\mathcal{L}$, which implies that it is a Fredholm operator with zero index. Now, the triviality of $\mathcal{N}(\mathcal{T})$ can be seen as an immediate consequence of the definition $\mathcal{T} = -4\pi A^*$ and lemma 3.5 and hence $\mathcal{T}$ maps continuously and bijectively $H^{1/2}(\partial D)$ onto $H^{-1/2}(\partial D)$.

For the reader's convenience, we collect the obtained results in the following corollary to theorem 3.3.

Corollary 3.7. *Assume that ω is not an interior transmission eigenvalue and k_{i}^2 is neither a Dirichlet eigenvalue nor a Neumann eigenvalue of $-\Delta$ in D. Then the ranges of G_2 and $(F^*F)^{1/4}$ coincide. Furthermore, the operators $(F^*F)^{-1/4}G_2$ and $G_2^{-1}(F^*F)^{1/4}$ are continuous isomorphisms from $H^{-1/2}(\partial D)$ onto $L^2(\Omega)$ and from $L^2(\Omega)$ onto $H^{-1/2}(\partial D)$, respectively.*

The combination of this corollary with theorem 3.2 and the fact that $\mathcal{R}(G) = \mathcal{R}(G_k)$, $k = 1, 2$, yields the main result of the factorization method, that is, the binary criterion which determines whether a given point is inside or outside the scattering obstacle D.

Theorem 3.8. *Assume that ω is not an interior transmission eigenvalue and k_{i}^2 is neither a Dirichlet eigenvalue nor a Neumann eigenvalue of $-\Delta$ in D. Then the scatterer D can be explicitly characterized as follows:*

$$\boldsymbol{z} \in D \quad \Longleftrightarrow \quad \Phi_{\mathrm{e}}^{\infty}(\cdot, \boldsymbol{z}) \in \mathcal{R}\big((F^*F)^{1/4}\big) \tag{64}$$

$$\Longleftrightarrow \quad [W(\boldsymbol{z})]^{-1} := \sum_{j=1}^{\infty} \frac{|\beta_j^{(\boldsymbol{z})}|^2}{|\lambda_j|} < \infty, \tag{65}$$

where $\beta_j^{(\boldsymbol{z})} := \big(\Phi_{\mathrm{e}}^{\infty}(\cdot, \boldsymbol{z}), \psi_j\big)_Y$ are the expansion coefficients of $\Phi_{\mathrm{e}}^{\infty}(\hat{\boldsymbol{x}}, \boldsymbol{z})$, $\hat{\boldsymbol{x}} \in \Omega$, with respect to the complete orthonormal system of eigenfunctions $\{\psi_j : j \in \mathbb{N}\}$ of the

compact, normal and injective operator F in Y and $\lambda_j \in \mathbb{C}$ are the corresponding eigenvalues.

Proof. Clearly, what remains is to prove the characterization (65). Let us first recall that the existence of a countable infinite number of eigenvalues of F is a direct consequence of the spectral theorem for compact normal operators (cf. [51]) and the completeness of the set of the corresponding eigenfunctions is attributed to the injectivity of F. Thus, there exists a countable set of eigenvalues $\lambda_j \in \mathbb{C}$ of F with $\lambda_j \neq 0$ for all $j \in \mathbb{N}$, and the corresponding orthonormal eigenelements $\{\psi_j : j \in \mathbb{N}\}$ with $F\psi_j = \lambda_j \psi_j$ form a complete orthonormal system in Y. Then, as a consequence of the obvious relation $F^*F\psi_j = |\lambda_j|^2\psi_j$ and the spectral decomposition of the compact, self-adjoint and positive operator $F^*F\colon Y \to Y$, one has that $(F^*F)^{1/4}\psi_j = \sqrt{|\lambda_j|}\psi_j$. Now, the characterization (64) suggests that a point $\boldsymbol{z} \in \mathbb{R}^3$ belongs to D if, and only if, the equation

$$\big((F^*F)^{1/4} g_{\boldsymbol{z}}\big)(\hat{\boldsymbol{x}}) = \Phi_{\mathrm{e}}^{\infty}(\hat{\boldsymbol{x}}, \boldsymbol{z}), \qquad \hat{\boldsymbol{x}} \in \Omega, \tag{66}$$

is solvable in the Hilbert space $Y = L^2(\Omega)$. Then, by an application of Picard's theorem [27], we have that (66) is solvable if, and only if, the series $\sum_{j=1}^{\infty} |\beta_j^{(\boldsymbol{z})}|^2/\mu_j^2$ is convergent, where μ_j are the singular values of $(F^*F)^{1/4}$, i.e., $\mu_j^2 = |\lambda_j|$, and in this case the solution of (66) is given by $g_{\boldsymbol{z}} = \sum_{j=1}^{\infty} (\beta_j^{(\boldsymbol{z})}/\sqrt{|\lambda_j|})\psi_j$. Thus, $\boldsymbol{z} \in D$ if, and only if, $\|g_{\boldsymbol{z}}\|_Y^2 = \sum_{j=1}^{\infty} |\beta_j^{(\boldsymbol{z})}|^2/|\lambda_j| < \infty$, which proves (65). □

4. Numerical Results

The explicit characterization of the unknown obstacle D in terms of the solvalibity of the linear first kind equation (66) in the Hilbert space Y, can now be used as a tool for exposing its support in an obvious way as the following simple procedure suggests:

(i) select a grid of 'sampling points' $\boldsymbol{z}$ in a region known *a priori* to contain D;

(ii) for each such point compute the value of the function $W(\boldsymbol{z})$ defined in (65), that is, the reciprocal of the squared norm of the solution $g_{\boldsymbol{z}}$ of (66);

(iii) determine the scatterer D as the location of those points $\boldsymbol{z}$ where the values of the function W become arbitrarily large (since the series fails to converge when $\boldsymbol{z} \notin D$).

In what follows, we briefly describe how to generate synthetic far-field data for a variety of surfaces in three dimensions and, additionally, its numerical approximation using the boundary element collocation method. Next, we will derive a series expansion for a sphere of radius $R > 0$ centered at the origin which we will use as a testing scenario to verify the correctness of the numerical approximation and show that we are able to obtain highly accurate far-field data due to superconvergence. Finally, we shortly explain the implementation of the factorization method and report the successful reconstruction of a variety of surfaces from the knowledge of the far-field data for different parameter settings.

4.1. Generation of synthetic far-field data

First, we derive the system of boundary integral equations to solve the problem (4)–(8). We make the ansatz of a combination of an acoustic double and single layer potential of the form

$$u^{\mathrm{sct}}(\boldsymbol{x}) = \mathrm{DL_e}\phi(\boldsymbol{x}) + \mathrm{SL_e}\psi(\boldsymbol{x}), \qquad \boldsymbol{x} \in \mathbb{R}^3\backslash\overline{D}, \tag{67}$$

$$u^{\mathrm{int}}(\boldsymbol{x}) = \tau\,\mathrm{DL_i}\phi(\boldsymbol{x}) + \tau\,\mathrm{SL_i}\psi(\boldsymbol{x}), \qquad \boldsymbol{x} \in D, \tag{68}$$

where ϕ and ψ are two unknown density functions defined on the surface ∂D. Letting the point $\boldsymbol{x}$ approach the boundary in (67) and (68) and using the jump relations leads to

$$u^{\mathrm{sct}} = \frac{1}{2}K_{\mathrm{e}}\phi + S_{\mathrm{e}}\psi + \frac{1}{2}\phi \quad \text{on} \quad \partial D,$$

$$u^{\mathrm{int}} = \frac{\tau}{2}K_{\mathrm{i}}\phi + \tau\,S_{\mathrm{i}}\psi - \frac{\tau}{2}\phi \quad \text{on} \quad \partial D.$$

Using the boundary condition $u^{\mathrm{sct}} - u^{\mathrm{int}} = -u^{\mathrm{inc}}$, with u^{inc} defined by (1), yields

$$\frac{1}{2}(1+\tau)\,\phi + \frac{1}{2}(K_{\mathrm{e}} - \tau\,K_{\mathrm{i}})\,\phi + (S_{\mathrm{e}} - \tau\,S_{\mathrm{i}})\,\psi = -u^{\mathrm{inc}}. \tag{69}$$

Taking the normal derivative in (67) and (68), letting the point x approach the boundary, and using the jump relations leads to

$$\frac{\partial u^{\mathrm{sct}}}{\partial \hat{\boldsymbol{\nu}}} = -R_{\mathrm{e}}\phi + \frac{1}{2}K'_{\mathrm{e}}\psi - \frac{1}{2}\psi \quad \text{on} \quad \partial D,$$

$$\frac{\partial u^{\mathrm{int}}}{\partial \hat{\boldsymbol{\nu}}} = -\tau\,R_{\mathrm{i}}\phi + \frac{\tau}{2}K'_{\mathrm{i}}\psi + \frac{\tau}{2}\psi \quad \text{on} \quad \partial D.$$

Using the boundary condition $\partial_{\hat{\boldsymbol{\nu}}}u^{\mathrm{sct}} - \tau^{-1}\partial_{\hat{\boldsymbol{\nu}}}u^{\mathrm{int}} = -\partial_{\hat{\boldsymbol{\nu}}}u^{\mathrm{inc}}$ yields

$$-\psi - (R_{\mathrm{e}} - R_{\mathrm{i}})\,\phi + \frac{1}{2}(K'_{\mathrm{e}} - K'_{\mathrm{i}})\,\psi = -\frac{\partial u^{\mathrm{inc}}}{\partial \hat{\boldsymbol{\nu}}}. \tag{70}$$

Equations (69) and (70) can be written in the form of a 2×2 system of boundary integral equations as follows

$$\left(\begin{bmatrix} \frac{1}{2}(1+\tau)I & 0 \\ 0 & -I \end{bmatrix} + \begin{bmatrix} \frac{1}{2}(K_{\mathrm{e}} - \tau\,K_{\mathrm{i}}) & S_{\mathrm{e}} - \tau\,S_{\mathrm{i}} \\ -(R_{\mathrm{e}} - R_{\mathrm{i}}) & \frac{1}{2}(K'_{\mathrm{e}} - K'_{\mathrm{i}}) \end{bmatrix}\right)\begin{bmatrix} \phi \\ \psi \end{bmatrix} = \begin{bmatrix} -u^{\mathrm{inc}} \\ -\frac{\partial u^{\mathrm{inc}}}{\partial \hat{\boldsymbol{\nu}}} \end{bmatrix}, \tag{71}$$

which has to be solved for the unknown density functions ϕ and ψ. The far-field pattern of (67) is given by

$$u^{\infty}(\hat{\boldsymbol{x}}) = \frac{1}{4\pi}\int_{\partial D}\left[\frac{\partial \mathrm{e}^{-\mathrm{i}k_{\mathrm{e}}\hat{\boldsymbol{x}}\cdot\boldsymbol{y}}}{\partial \hat{\boldsymbol{\nu}}(\boldsymbol{y})}\phi(\boldsymbol{y}) + \mathrm{e}^{-\mathrm{i}k_{\mathrm{e}}\hat{\boldsymbol{x}}\cdot\boldsymbol{y}}\psi(\boldsymbol{y})\right]\mathrm{d}s(\boldsymbol{y}), \qquad \hat{\boldsymbol{x}} \in \Omega. \tag{72}$$

Note that we used the layer ansatz, because all entries in (71) are integral operators with weakly singular kernel for which numerical approximations can be constructed. Furthermore, the derivation is similar to the one presented in [42] by the third author. We use the boundary element collocation method to solve (71) numerically (see [42, Chapter 5] for a detailed description). After obtaining the unknown densities at the collocation nodes, we can numerically evaluate (72) to obtain the far-field pattern. In a similar fashion as in [42, Chapter 6], we will be able to show a rate of convergence

of almost four using quadratic basis functions, thus leading to superconvergence. Note that the numerical program developed by the third author (see [39]) is an extension of BIEPACK (boundary integral equation package for the solution of integral equations of the second kind arising from the Laplace equation) developed by Atkinson (see [5]) which has been recently used in a variety of problems dealing with the Helmholtz equation (see [35, 40, 41, 42, 43, 44] among others).

4.2. Series expansion for a sphere

In this section, we derive a series expansion for a sphere of radius $R > 0$ centered at the origin. Note that j_n denotes the spherical Bessel function of the first kind of order n, $h_n^{(1)}$ the spherical Hankel function of the first kind of order n, and P_n is the Legendre polynomial of order n. With the notation $\boldsymbol{x} = r\hat{\boldsymbol{x}}$, $r > 0$ and $\hat{\boldsymbol{x}} \in \Omega$ we have

$$u^{\mathrm{sct}}(r\hat{\boldsymbol{x}}) = \sum_{n=0}^{\infty} \sum_{m=-n}^{n} a_n^m h_n^{(1)}(k_{\mathrm{e}} r) Y_n^m(\hat{\boldsymbol{x}}) \,, \quad r > R \,,$$

in the exterior (see [16, Theorem 2.14]). In the interior we have

$$u^{\mathrm{int}}(r\hat{\boldsymbol{x}}) = \sum_{n=0}^{\infty} \sum_{m=-n}^{n} b_n^m j_n(k_{\mathrm{i}} r) Y_n^m(\hat{\boldsymbol{x}}) \,, \quad r < R \,.$$

Using the Jacobi-Anger expansion of the incident field yields

$$u^{\mathrm{inc}}(r\hat{\boldsymbol{x}}; \hat{\boldsymbol{d}}) = \sum_{n=0}^{\infty} \sum_{m=-n}^{n} 4\pi \mathrm{i}^n j_n(k_{\mathrm{e}} r) Y_n^m(\hat{\boldsymbol{x}}) \overline{Y_n^m(\hat{\boldsymbol{d}})} \,.$$

Using the boundary condition on the sphere $r = R$ yields the following system of two equations for the unknown coefficients a_n^m and b_n^m:

$$\begin{bmatrix} h_n^{(1)}(k_{\mathrm{e}} R) & -j_n(k_{\mathrm{i}} R) \\ k_{\mathrm{e}} h_n^{(1)'}(k_{\mathrm{e}} R) & -\tau^{-1} k_{\mathrm{i}} j_n'(k_{\mathrm{i}} R) \end{bmatrix} \begin{bmatrix} a_n^m \\ b_n^m \end{bmatrix} = \begin{bmatrix} -4\pi \mathrm{i}^n j_n(k_{\mathrm{e}} R) \overline{Y_n^m(\hat{\boldsymbol{d}})} \\ -4\pi \mathrm{i}^n j_n'(k_{\mathrm{e}} R) \overline{Y_n^m(\hat{\boldsymbol{d}})} k_{\mathrm{e}} \end{bmatrix} .$$

Solving this system for a_n^m gives

$$a_n^m = -4\pi \mathrm{i}^n \overline{Y_n^m(\hat{\boldsymbol{d}})} \frac{k_{\mathrm{i}} j_n'(k_{\mathrm{i}} R) j_n(k_{\mathrm{e}} R) - \tau k_{\mathrm{e}} j_n'(k_{\mathrm{e}} R) j_n(k_{\mathrm{i}} R)}{k_{\mathrm{i}} j_n'(k_{\mathrm{i}} R) h_n^{(1)}(k_{\mathrm{e}} R) - \tau k_{\mathrm{e}} h_n^{(1)'}(k_{\mathrm{e}} R) j_n(k_{\mathrm{i}} R)} \,.$$

The far-field pattern of u^{sct} is given by (see [16, Theorem 2.15])

$$\begin{aligned} u^{\infty}(\hat{\boldsymbol{x}}) &= \frac{1}{k_{\mathrm{e}}} \sum_{n=0}^{\infty} \frac{1}{\mathrm{i}^{n+1}} \sum_{m=-n}^{m} a_n^m Y_n^m(\hat{\boldsymbol{x}}) \\ &= \frac{\mathrm{i}}{k_{\mathrm{e}}} \sum_{n=0}^{\infty} (2n+1) \frac{k_{\mathrm{i}} j_n'(k_{\mathrm{i}} R) j_n(k_{\mathrm{e}} R) - \tau k_{\mathrm{e}} j_n'(k_{\mathrm{e}} R) j_n(k_{\mathrm{i}} R)}{k_{\mathrm{i}} j_n'(k_{\mathrm{i}} R) h_n^{(1)}(k_{\mathrm{e}} R) - \tau k_{\mathrm{e}} h_n^{(1)'}(k_{\mathrm{e}} R) j_n(k_{\mathrm{i}} R)} P_n(\hat{\boldsymbol{x}} \cdot \hat{\boldsymbol{d}}) \,, \end{aligned} \tag{73}$$

where the last step follows from the addition theorem for spherical harmonics (see [16, Theorem 2.8]). In the following, we create 66 incident waves and measure the far-field pattern in the same directions (see [35, Appendix A.1] for the generation of the 66 waves). This gives our set of data f_{ij} with $i, j = 1, \ldots, 66$, which we collect in a matrix, say $F \in \mathbb{C}^{66 \times 66}$. Due to the series expansion (73), we are able to compare our numerical

approximation of the far-field pattern. The error between the calculated solution f_{ij} and the 'true' far-field pattern $u^\infty(\hat{\boldsymbol{x}}_i, \hat{\boldsymbol{d}}_j)$ at the point $\hat{\boldsymbol{x}}_i \in \Omega$ corresponding to direction of incidence $\hat{\boldsymbol{d}}_j \in \Omega$ is denoted by $\mathcal{E}_n(\hat{\boldsymbol{x}}_i, \hat{\boldsymbol{d}}_j)$. More precisely, we have that

$$\mathcal{E}_n(\hat{\boldsymbol{x}}_i, \hat{\boldsymbol{d}}_j) = \left| u^\infty(\hat{\boldsymbol{x}}_i, \hat{\boldsymbol{d}}_j) - f_{ij} \right| .$$

The estimated order of convergence is defined by

$$\mathrm{EOC} = \log\left(\max_{i,j} \left\{ \mathcal{E}_n(\hat{\boldsymbol{x}}_i, \hat{\boldsymbol{d}}_j) \right\} / \max_{i,j} \left\{ \mathcal{E}_{4n}(\hat{\boldsymbol{x}}_i, \hat{\boldsymbol{d}}_j) \right\} \right) / \log(2) .$$

In table 1 we report the maximal error and the estimated order of convergence (EOC) for $k_\mathrm{e} = 2$, $k_\mathrm{i} = 1$, $\tau = 1/2$, and $R = 1$, where n denotes the number of faces of the triangulation and the number of collocation points is denoted by n_v. Using quadratic

	Quadratic interpolation				
n (n_v)	$\max_{i,j} \mathcal{E}_n(\hat{\boldsymbol{x}}_i, \hat{\boldsymbol{d}}_j)$	EOC	n (n_v)	$\max_{i,j} \mathcal{E}_n(\hat{\boldsymbol{x}}_i, \hat{\boldsymbol{d}}_j)$	EOC
4 (24)	2.3883D-01	2.99	8 (48)	3.4775D-02	4.82
16 (96)	3.0120D-02	5.59	32 (192)	1.2316D-03	6.58
64 (384)	6.2361D-04	5.51	128 (768)	1.2885D-05	3.63
256 (1536)	1.3656D-05		512 (3072)	1.0405D-06	

Table 1. Far-field pattern errors for a sphere with $R = 1$ and the parameters $k_\mathrm{e} = 2$, $k_\mathrm{i} = 1$, and $\tau = 1/2$.

interpolation usually leads to a rate of convergence of order three; i.e., $\mathcal{O}(\hat{\delta}_n^3)$ (see [42, Theorem 5.1]) where $\hat{\delta}_n$ is the mesh size of the parametrization domain. More precisely, $\hat{\delta}_n$ is the maximum diameter of the n elements that triangulate the parametrization domain (see [42, p. 335] for the definition). As shown in [42, Theorem 6.1], we are able to prove theoretically a convergence rate of almost four; i.e., $\mathcal{O}(\hat{\delta}_n^4 \log\left(\hat{\delta}_n^{-1}\right))$. Although the estimated rate of convergence is slightly varying, one can observe that we achieve numerically a rate of convergence of almost four which in turn shows that our boundary element collocation solver is able to correctly produce highly accurate far-field data. It is noted that other parameter choices lead to similar results.

4.3. Reconstruction of a variety of surfaces

We proceed by demonstrating that one is able to successfully reconstruct a variety of different surfaces with the factorization method from the knowledge of the far-field pattern. The surfaces under consideration are shown in figure 1; specifically, their triangulation is depicted.

The first surface is a unit sphere. The second surface is an ellipsoid with semi-axes $(1, 1, 6/5)$. The third surface is peanut-shaped and given in spherical coordinates via $x = \varrho \sin(\phi)\cos(\theta)$, $y = \varrho \sin(\phi)\sin(\theta)$, and $z = \varrho\cos(\phi)$ with $\varrho^2 = 9\left\{\cos^2(\phi) + \sin^2(\phi)/4\right\}/4$. The fourth surface is acorn-shaped and parametrically

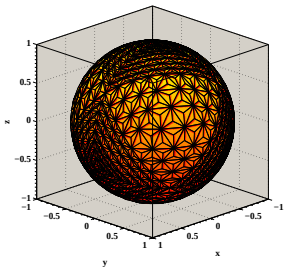

(a) Triangulation of a unit sphere with 512 faces.

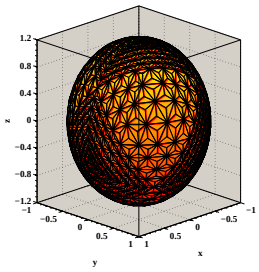

(b) Triangulation of an ellipsoidal surface with 512 faces.

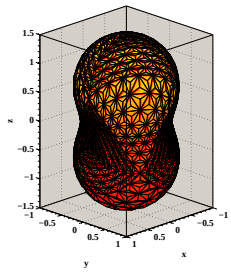

(c) Triangulation of a peanut-shaped surface with 512 faces.

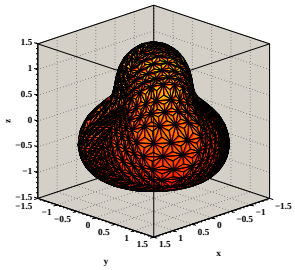

(d) Triangulation of an acorn-shaped surface with 512 faces.

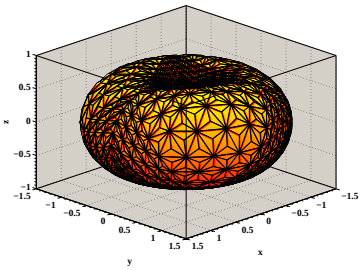

(e) Triangulation of a cushion-shaped surface with 512 faces.

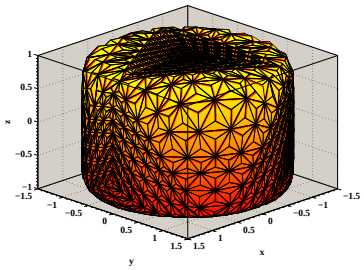

(f) Triangulation of a round short cylinder-shaped surface with 512 faces.

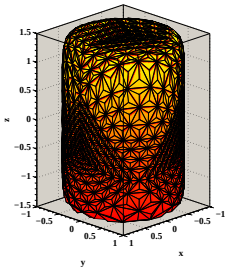

(g) Triangulation of a round long cylinder-shaped surface with 512 faces.

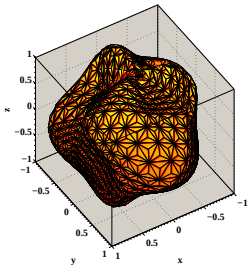

(h) Triangulation of a bumpy sphere with 512 faces.

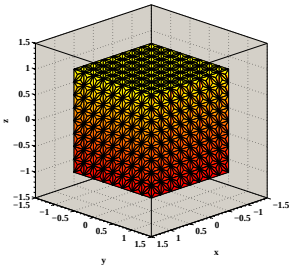

(i) Triangulation of a cube with 768 faces.

Figure 1. Different surfaces under consideration.

given by $\varrho^2 = 9\{17/4 + 2\cos(3\phi)\}/25$. The fifth surface is a cushion-shaped surface and represented by $\varrho = 1 - \cos(2\phi)/2$. The sixth and seventh surface are a round short and long cylinder given by $\varrho^{10} = 1/((2\sin(\phi)/3)^{10} + \cos^{10}(\phi))$ and $\varrho^{10} = 1/((2\cos(\phi)/3)^{10} + \sin^{10}(\phi))$, respectively. The eighth surface is a bumpy sphere arising in tumor growth modeling, which is given by $\varrho = 1 + \sin(3\phi)\sin(3\theta)/5$. The last surface is a cube centered at the origin with edge length two.

Note that we use 3072 collocation nodes for all surfaces with the exception of the cube, where we use 4608 collocation nodes and the parameters $N_S = 128$ and $N_{NS} = 4$ to generate the synthetic far-field data.

The implementation of the factorization method for reconstructing the surfaces is

rather straightforward and easy (see, also, [34] for a description). First, define a grid $\mathcal{G}$, say a cube $\mathcal{C} = [-t, +t]^3$ with some parameter $t > 0$, with N equidistant points in each of the three directions. Second, compute a singular value decomposition of the given matrix $F = U\Lambda V^* \in \mathbb{C}^{66\times 66}$, which contains the far-field data. Note that we are not necessarily restricted to the size of 66. Third, for each point $\boldsymbol{z}$ from the grid ($N \times N \times N$ values) we have to compute the expansion coefficients of the expression $r_{\boldsymbol{z}} = (\exp(-\mathrm{i}k_\mathrm{e}\boldsymbol{z}\cdot\hat{\boldsymbol{d}}_j))_{j=1,\ldots,66} \in \mathbb{C}^{66}$ with respect to the columns of V by

$$\beta_l^{(\boldsymbol{z})} = \sum_{j=1}^{66} V_{j,l}\, \mathrm{e}^{-\mathrm{i}k_\mathrm{e}\boldsymbol{z}\cdot\hat{\boldsymbol{d}}_j}\,, \quad l = 1, \ldots, 66\,,$$

which is a simple matrix-vector multiplication $\rho^{(\boldsymbol{z})} := V^{\mathrm{T}} r_{\boldsymbol{z}}$ of V^{T} and $r_{\boldsymbol{z}}$. Finally, we calculate

$$W(\boldsymbol{z}) = \left[\sum_{l=1}^{66} \frac{|\beta_l^{(\boldsymbol{z})}|^2}{|\lambda_l|}\right]^{-1}$$

for the indicator function in (65). Then, the isosurface of the map $\boldsymbol{z} \mapsto W(\boldsymbol{z})$ will be plotted for an appropriately selected cut-off value, say γ, using the unit sphere as the 'calibration' scatterer.

As a first parameters choice, we select $k_\mathrm{e} = 2$, $k_\mathrm{i} = 1$, and $\tau = 1/2$. Recall that the values of $W(\boldsymbol{z})$ should be much larger for $\boldsymbol{z} \in D$ than those in the exterior. We plot the slice $W(x_i, 0, 0)$ for $i = 1, \ldots, 55$ for the unit sphere to get an idea of how to choose the threshold parameter γ. As we can see in figure 2, the threshold parameter should be chosen between 4 and 7; we choose $\gamma = 6$. The reconstructions of all nine surfaces

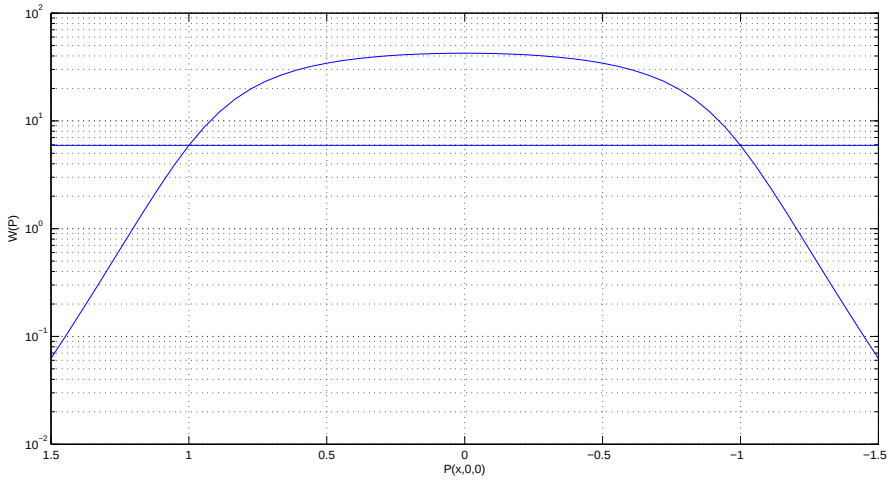

Figure 2. The slice $W(x_i, 0, 0)$ for $i = 1, \ldots, 55$ of W for the far-field data of a sphere of radius one.

are shown in figure 3. Note that we have used $t = 1.5$ and $N = 55$ for all surfaces with the exception of the cylinders, where we have used $t = 2$ and $N = 73$.

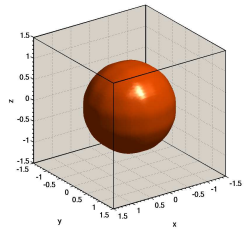

(a) Reconstructed surface of a unit sphere.

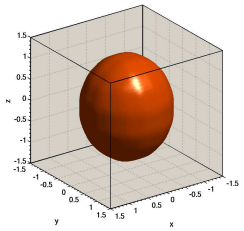

(b) Reconstructed ellipsoidal surface.

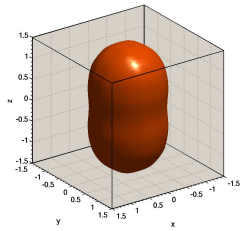

(c) Reconstructed peanut-shaped surface.

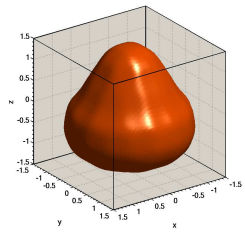

(d) Reconstructed acorn-shaped surface.

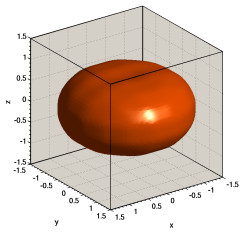

(e) Reconstructed cushion-shaped surface.

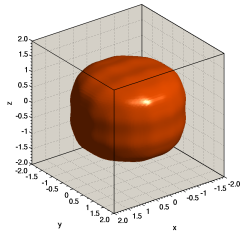

(f) Reconstructed round short cylinder-shaped surface.

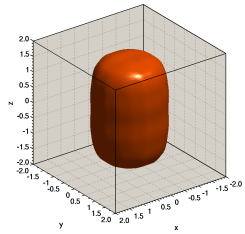

(g) Reconstructed round long cylinder-shaped surface.

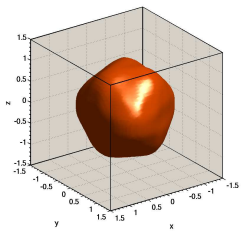

(h) Reconstructed surface of a bumpy sphere.

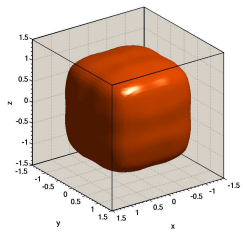

(i) Reconstructed surface of a cube.

Figure 3. Nine reconstructed surfaces with the factorization method using $\gamma = 6$. Parameters are $k_e = 2$, $k_i = 1$, and $\tau = 1/2$.

As we can observe, the reconstruction of all nine surfaces are quiet accurate. Interestingly, the method also works for piecewise smooth surfaces although this is not justified from the theoretical point of view. The reconstruction of the bumpy sphere is very smooth, but the trend is clear. Hence, we have a clear indication that the $(F^*F)^{1/4}$-factorization method is justified not only from the theoretical but from the computational point of view.

Needless to say that the reconstruction's quality depends on the amount of noise in the far-field data. Due to the generation of synthetic data by the forward solver, we actually, already, deal with noisy far-field data. To quantify this, one may employ the 'normality' criterion. More precisely, after measuring $\|F^*F - FF^*\|_2$ using the matrix spectral norm, we acquire the following values for the previous nine surfaces: 0.5833, 1.3546, 2.9651, 5.8632, 7.0939, 21.6075, 11.0284, 0.8023, 4.2491, respectively.

Next, we again consider the acorn-shaped surface and add Gaussian white noise to the real and imaginary part of F of various levels. The obtained reconstructions for various white noise scenarios are shown in figure 4, where we used $t = 2$ and $N = 73$. As one might expect, an increase in the noise level on the far-field data results in a

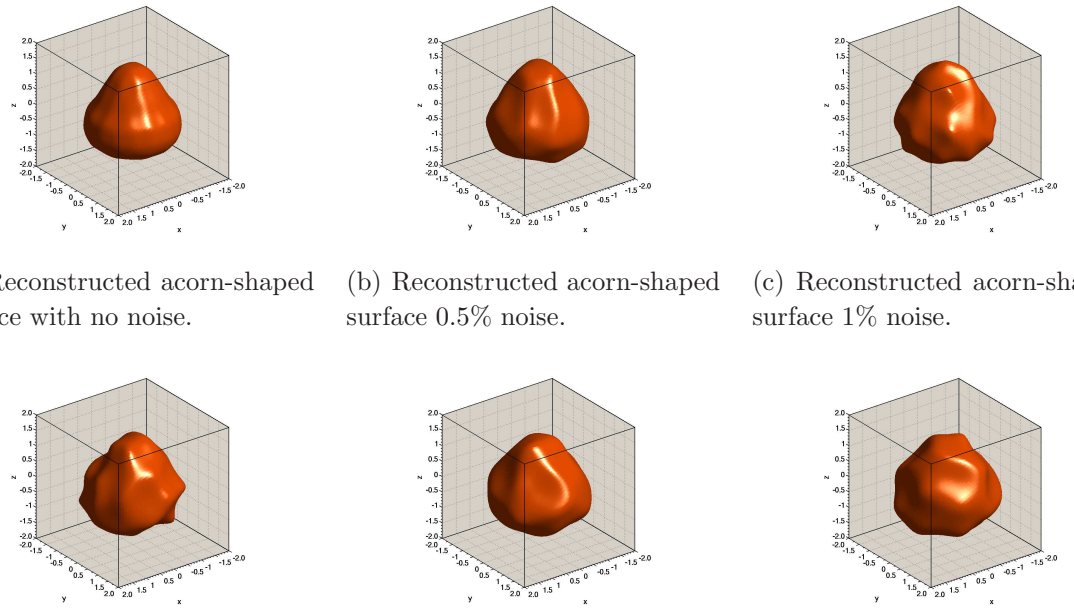

(a) Reconstructed acorn-shaped surface with no noise.

(b) Reconstructed acorn-shaped surface 0.5% noise.

(c) Reconstructed acorn-shaped surface 1% noise.

(d) Reconstructed acorn-shaped surface 1.5% noise.

(e) Reconstructed acorn-shaped surface 2% noise.

(f) Reconstructed acorn-shaped surface 5% noise.

Figure 4. The reconstructed acorn-shaped surface with the factorization method using $\gamma = 6$ for various noise levels. Parameters are $k_e = 2$, $k_i = 1$, and $\tau = 1/2$.

deterioration of the reconstruction's quality. It should be noted, however, that the region containing the unknown scatterer is clearly identified by the method in all cases.

We now turn our attention to examining the influence of the choice of the threshold parameter γ on the method's performance. By virtue of figure 5, where the reconstruction of the acorn-shaped surface for different values of γ is depicted, we clearly deduce that the choice of the threshold parameter is crucial, since different choices lead to good or less accurate reconstructions. In the same spirit, for a different set of parameters, namely $k_e = 2$, $k_i = 1$, and $\tau = 2$, we again look at the slice $W(x_i, 0, 0)$ for the unit sphere. The suggested choice of γ should now be 4. Figure 6 illustrates the reconstruction of a selected choice of obstacles for the parameters $k_e = 2$, $k_i = 1$, and $\tau = 2$. As one can observe, the first three surfaces are reconstructed satisfactorily whereas the last three surfaces are not that well reconstructed.

Of course, one can, usually, achieve an increase of the reconstruction's quality by employing a greater number of incidence and observation directions. This is revealed in figure 7, where we show the reconstruction of the previous six surfaces (see figure 6 for a comparison) for 258 incident waves and the threshold parameter chosen as $\gamma = 4$. As one easily confirms, the reconstructions are of higher accuracy for increasing number

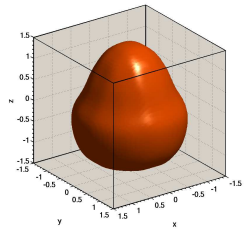

(a) Reconstructed acorn-shaped surface for $\gamma = 3$.

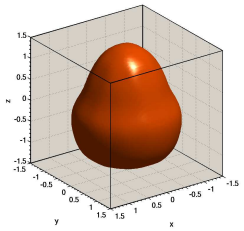

(b) Reconstructed acorn-shaped surface for $\gamma = 3.5$.

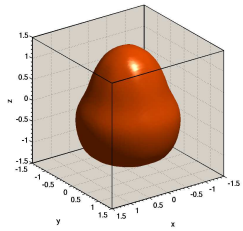

(c) Reconstructed acorn-shaped surface for $\gamma = 4$.

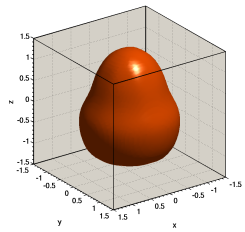

(d) Reconstructed acorn-shaped surface for $\gamma = 4.5$.

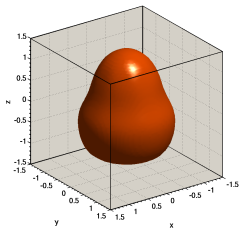

(e) Reconstructed acorn-shaped surface for $\gamma = 5$.

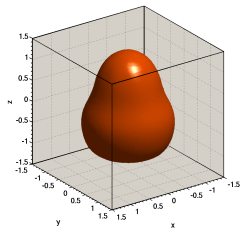

(f) Reconstructed acorn-shaped surface for $\gamma = 5.5$.

Figure 5. Reconstructed surfaces with the factorization method using various γ for the acorn-shaped surface. Parameters are $k_e = 2$, $k_i = 1$, and $\tau = 1/2$.

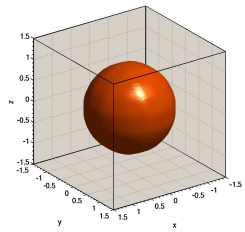

(a) Reconstructed surface of a unit sphere.

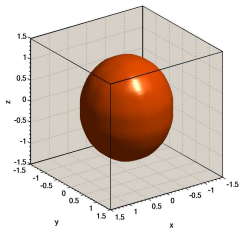

(b) Reconstructed ellipsoidal surface.

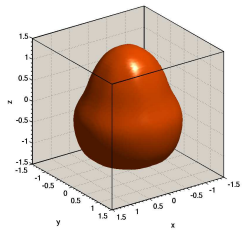

(c) Reconstructed acorn-shaped surface.

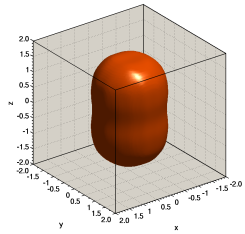

(d) Reconstructed round long cylinder-shaped surface.

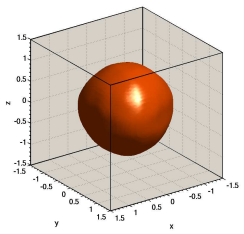

(e) Reconstructed surface of a bumpy sphere.

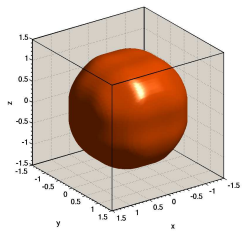

(f) Reconstructed surface of a cube.

Figure 6. Six reconstructed surfaces with the factorization method using $\gamma = 4$. Parameters are $k_e = 2$, $k_i = 1$, and $\tau = 2$.

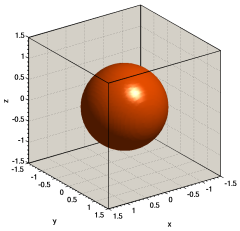

(a) Reconstructed surface of a unit sphere.

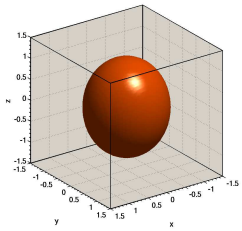

(b) Reconstructed ellipsoidal surface.

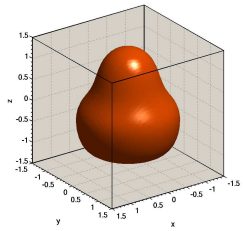

(c) Reconstructed acorn-shaped surface.

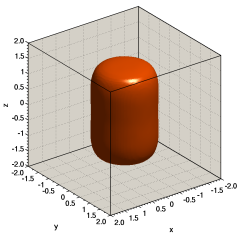

(d) Reconstructed round long cylinder-shaped surface.

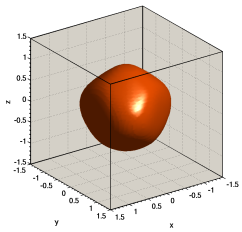

(e) Reconstructed surface of a bumpy sphere.

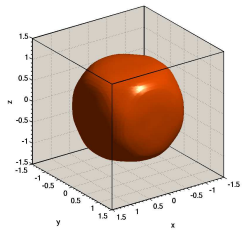

(f) Reconstructed surface of a cube.

Figure 7. Six reconstructed surfaces with the factorization method using $\gamma = 4$ and $F \in \mathbb{C}^{258\times 258}$. Parameters are $k_e = 2$, $k_i = 1$, and $\tau = 2$.

of incidence and observation directions compared to the previous reconstructions. This is evident for the acorn-shaped and the round long-cylinder shaped surfaces. However, the reconstruction of the bumpy sphere, although certainly better, is not that good. Finally, the surface of the cube appears, also, to be more accurately reconstructed.

Next, we further investigate the quality of the reconstructions for the peanut-shaped, acorn-shaped, and cushion-shaped surfaces for varying number of incidence and observation directions, aiming at identifying a 'lower bound' for this number. In figure 8, we provide reconstructions for those three surfaces, where we have used the parameters $k_e = 2$, $k_i = 1$, $\tau = 1/2$, $t = 1.5$, and $N = 55$. We observe that we need more than 34 incident waves and observation directions to obtain a good reconstruction for all three surfaces under consideration. A descent reconstruction is obtained for 34 incident waves and observation directions. Using 18 incident waves and observation directions results in poor reconstructions, even for the increased values $t = 2$ and $N = 73$. Of course, our criterion for assessing the reconstructions' quality is the human visual perception, since there is a lack of a quantitative criterion to measure the quality of the reconstructions.

In a next step, we provide some numerical examples, which aim at demonstrating the ability of the factorization method to deliver reconstructions with no *a priori* information about the number of connected components of the unknown scatterer. First, we consider an example with two scatterers. To create the far-field, we use the following heuristic approach. We separately compute the far-field for a cube centered at $(0, 0, 3)$ with edge length two and for a unit sphere centered at $(0, 0, -3)$ using 66 directions

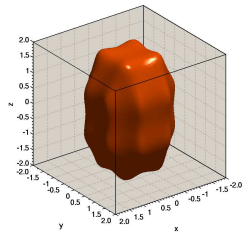

(a) Peanut-shaped surface with $F \in \mathbb{C}^{18\times 18}$.

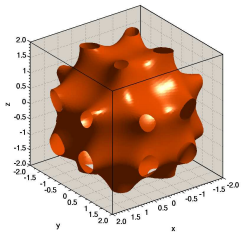

(b) Acorn-shaped surface with $F \in \mathbb{C}^{18\times 18}$.

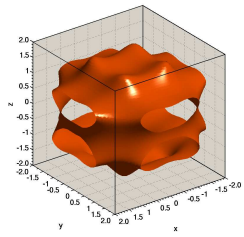

(c) Cushion-shaped surface with $F \in \mathbb{C}^{18\times 18}$.

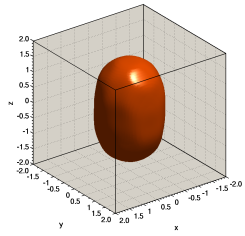

(d) Peanut-shaped surface with $F \in \mathbb{C}^{34\times 34}$.

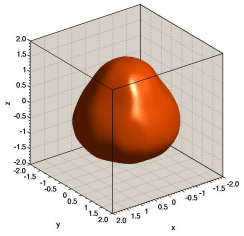

(e) Acorn-shaped surface with $F \in \mathbb{C}^{34\times 34}$.

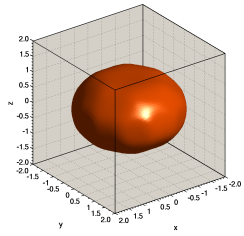

(f) Cushion-shaped surface with $F \in \mathbb{C}^{34\times 34}$.

Figure 8. Three reconstructed surfaces with the factorization method using $\gamma = 6$ for varying number of incidence and observation directions. Parameters are $k_e = 2$, $k_i = 1$, and $\tau = 1/2$.

of incidence and of observation and the parameters $k_e = 2$, $k_i = 1$, and $\tau = 1/2$. We subsequently form the superposition of the two far-field patterns and use it as the forward data for the factorization method algorithm. Although a heuristic and mathematically unjustified approach which, of course, ignores both multiple scattering effects and all interactions among the members of the cluster, we have decided to adopt it as an 'ultimate proof' that the method indeed works with no *a priori* information♯. Indeed, this is the case in figure 9(a). Additionally, we provide a second example in figure 9(b) with an acorn centered at the origin and a unit sphere centered at $(0, 0, -5)$. In both cases, we are able to reconstruct satisfactorily the two distinct obstacles. However, one observes that the reconstructions of the sphere and the cube, depicted in figure 9(a), seem to 'attract' each other, which is, also, true for the reconstructions in figure 9(b). To interpret this behaviour, one should take into account that the 'real' distance between the two objects (lower cube face and top of the sphere) is 4 units, which is very close to the wavelength $\lambda_e = \pi$, in the host medium. Not much can be expected for distances smaller than a wavelength. This is actually revealed in figure 10, where we have used the first example (figure 9(a)) and inserted an acorn-shaped obstacle between the cube and the sphere. Therein, the three obstacles, being too close to each other, tend to get merged. (Note that for the reconstruction of multiple scatterers, we have used $t = 2$

♯ It is noted that such an approach has already been used by pioneers in the field (see, for example, [38, p. 104] for generating far-field data for two open arcs).

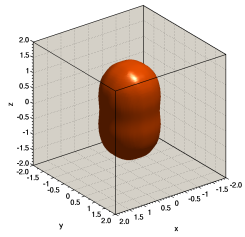

(g) Peanut-shaped surface with $F \in \mathbb{C}^{66\times 66}$.

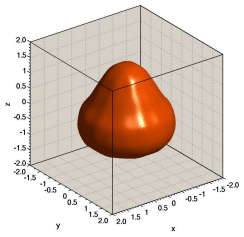

(h) Acorn-shaped surface with $F \in \mathbb{C}^{66\times 66}$.

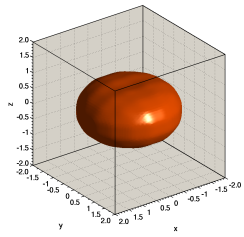

(i) Cushion-shaped surface with $F \in \mathbb{C}^{66\times 66}$.

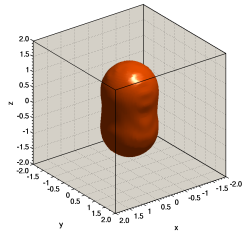

(j) Peanut-shaped surface with $F \in \mathbb{C}^{130\times 130}$.

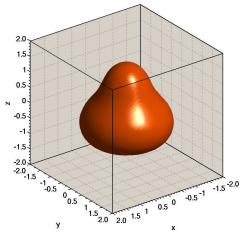

(k) Acorn-shaped surface with $F \in \mathbb{C}^{130\times 130}$.

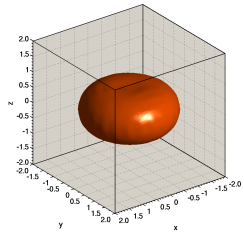

(l) Cushion-shaped surface with $F \in \mathbb{C}^{130\times 130}$.

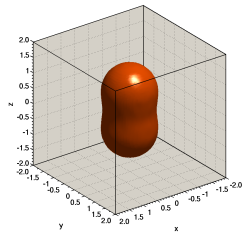

(m) Peanut-shaped surface with $F \in \mathbb{C}^{258\times 258}$.

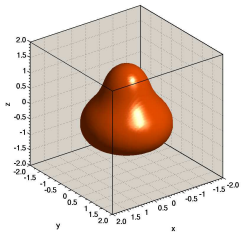

(n) Acorn-shaped surface with $F \in \mathbb{C}^{258\times 258}$.

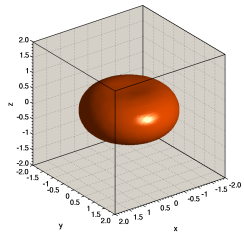

(o) Cushion-shaped surface with $F \in \mathbb{C}^{258\times 258}$.

Figure 8. Three reconstructed surfaces with the factorization method using $\gamma = 6$ for varying number of incidence and observation directions. Parameters are $k_e = 2$, $k_i = 1$, and $\tau = 1/2$.

with $N = 73$ in x- and y-direction and $N = 163$ in the z-direction.)

All the numerical reconstructions presented so far, have been obtained by solving a discretized version of the far-field equation (66), which is, of course, inherently ill-posed due to the compactness of the far-field operator. Alternatively, one may obtain an approximate solution of the continuous problem by employing an appropriate regularization scheme. In what follows, we investigate the use of a regularized version of the far-field equation according to the Tikhonov-Morozov regularization scheme [50, 54]. Thus, at the discrete level, instead of considering

$$\|g_{\boldsymbol{z}}\|^2 = \sum_{l=1}^{66} \frac{|\beta_l^{(\boldsymbol{z})}|^2}{|\lambda_l|} := \frac{1}{W(\boldsymbol{z})},$$

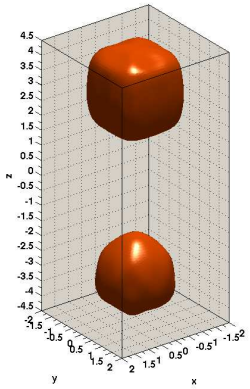

(a) Reconstructed cube of edge length two and unit sphere with $F \in \mathbb{C}^{66\times 66}$.

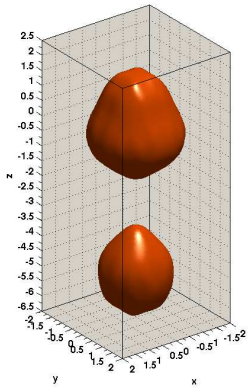

(b) Reconstructed acorn-shaped surface and unit sphere with $F \in \mathbb{C}^{66\times 66}$.

Figure 9. Two simultaneously reconstructed surfaces with the factorization method using $\gamma = 6$. Parameters are $k_e = 2$, $k_i = 1$, and $\tau = 1/2$.

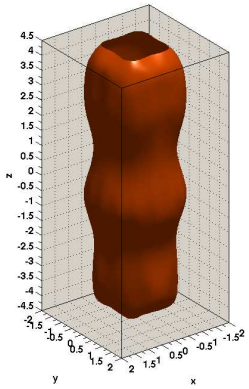

(a) Reconstructed cube of edge length two, acorn-shaped surface, and unit sphere with $F \in \mathbb{C}^{66\times 66}$.

Figure 10. Three simultaneously reconstructed surfaces with the factorization method using $\gamma = 6$. Parameters are $k_e = 2$, $k_i = 1$, and $\tau = 1/2$.

we compute

$$\|g_{\boldsymbol{z},\alpha}\|^2 = \sum_{l=1}^{66} \frac{|\lambda_l|}{(\alpha + |\lambda_l|)^2} |\beta_l^{(\boldsymbol{z})}|^2 := \frac{1}{W_\alpha(\boldsymbol{z})},$$

where the regularization parameter α is determined for each point $\boldsymbol{z}$ on the selected grid as the unique zero of the discrepancy function

$$f(\alpha) = \sum_{l=1}^{66} \frac{\alpha^2 - \delta^2|\lambda_l|}{(\alpha + |\lambda_l|)^2} |\beta_l^{(\boldsymbol{z})}|^2,$$

for some known estimate δ for the error in the far-field matrix. We use the following procedure to corrupt the far-field matrix in such a way that $\|F - F_\delta\|_2 \leqslant \delta$ can be

ensured: Let N_R and N_I be two random matrices with entries uniformly distributed in the interval $[-1, 1]$. For a given ϵ, we define the perturbed matrix F_δ by

$$F_\delta := F + \epsilon\,(N_R + \mathrm{i}N_I)\,F.$$

Hence, we can always choose ϵ so that $\|F - F_\delta\|_2 \leqslant \delta$ is guaranteed for some δ. With this δ at hand, we can then compute the regularization parameter α for each point $\boldsymbol{z}$ in the grid. It is to be noted, however, that this does not include the error in the far-field data due to the forward solver, which could be much larger than the error due to the artificially introduced random noise. In other words, the whole approach is very likely to underestimate the 'true' error in the far-field data.

In figures 11 and 12, we show the reconstruction of the acorn-shaped surface for $\delta = 1\%$ and $\delta = 5\%$, respectively, using both the unregularized and the regularized version of the far-field equation (i.e., plots of $W(\boldsymbol{z})$ and $W_\alpha(\boldsymbol{z})$, respectively) for the parameters $k_\mathrm{e} = 2$, $k_\mathrm{i} = 1$, and $\tau = 1/2$. For completeness, we also include isosurface plots for the map $\boldsymbol{z} \mapsto \alpha(\boldsymbol{z})$, after adjusting appropriately the threshold parameter γ.

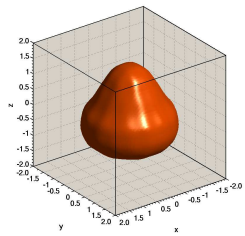

(a) Isosurface of $W(z)$ with threshold $\gamma = 6$.

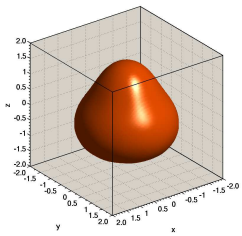

(b) Isosurface of $W_\alpha(z)$ with threshold $\gamma = 6$.

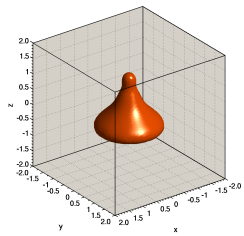

(c) Isosurface of $\alpha(z)$ with threshold $\gamma = 0.01$.

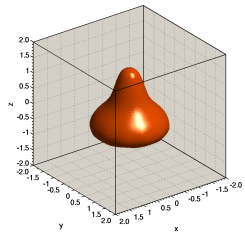

(d) Isosurface of $\alpha(z)$ with threshold $\gamma = 0.005$.

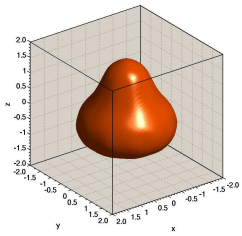

(e) Isosurface of $\alpha(z)$ with threshold $\gamma = 0.001$.

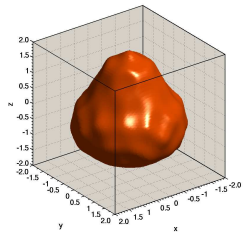

(f) Isosurface of $\alpha(z)$ with threshold $\gamma = 0.0005$.

Figure 11. Reconstruction of the acorn-shaped surface using the unregularized and regularized version of the far-field equation with 66 incident waves and observation directions using $\delta = 1\%$. Parameters are $k_\mathrm{e} = 2$, $k_\mathrm{i} = 1$, and $\tau = 1/2$.

Figures 11 and 12, clearly demonstrate that a stable reconstruction can be obtained upon using the regularized far-field equation. Interestingly, we are also able to exploit the mapping $\boldsymbol{z} \mapsto \alpha(\boldsymbol{z})$ to get a reconstruction of the unknown scatterer's surface (see, e.g., figure 11(e)), which sometimes appears even better than both the regularized and unregularized reconstructions. However, note that the employment of a regularization

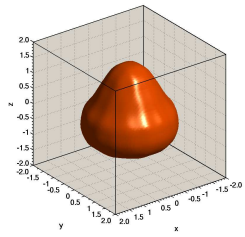

(a) Isosurface of $W(z)$ with threshold $\gamma = 6$.

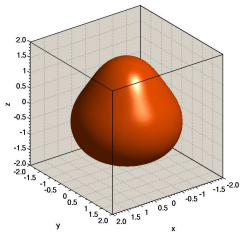

(b) Isosurface of $W_\alpha(z)$ with threshold $\gamma = 6$.

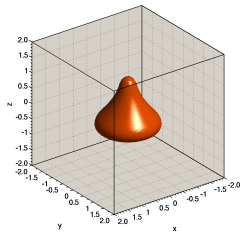

(c) Isosurface of $\alpha(z)$ with threshold $\gamma = 0.1$.

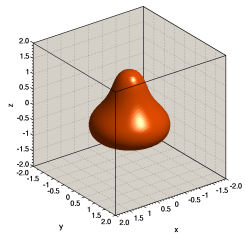

(d) Isosurface of $\alpha(z)$ with threshold $\gamma = 0.05$.

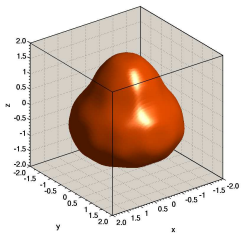

(e) Isosurface of $\alpha(z)$ with threshold $\gamma = 0.01$.

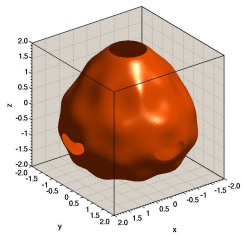

(f) Isosurface of $\alpha(z)$ with threshold $\gamma = 0.005$.

Figure 12. Reconstruction of the acorn-shaped surface using the unregularized and regularized version of the far-field equation with 66 incident waves and observation directions using $\delta = 5\%$. Parameters are $k_e = 2$, $k_i = 1$, and $\tau = 1/2$.

scheme for solving the far-field equation does not lead to superior reconstructions compared with those obtained without regularization. This has also been observed in [14]. In fact, the regularized reconstruction appears to be, overall speaking, a little smoother than the unregularized one.

5. Summary

In this study, the problem of reconstructing three-dimensional acoustically penetrable obstacles in an infinite acoustic medium from far-field measurements is investigated by means of the factorization method. To this end, a three-dimensional inverse analysis of acoustic plane waves scattered by an obstacle is formulated as a linear equation of the first kind whose solvability offers a binary criterion which determines whether a given point is inside or outside the scattering obstacle. For a rigorous approach to the problem, the theoretical foundation of the factorization method has been systematically extended to the penetrable scatterer case in far-field acoustics by deriving an appropriate factorization of the far-field operator with the participating operators disposing specific properties. The theoretical investigation of the method is complemented by numerical examples which exploit generated synthetic far-field data for a variety of surfaces in three dimensions. The elaborated numerical reconstructions reveal that the factorization method is capable of effectively identifying both connected and disconnected scatterers

in terms of their location and geometry for various selections of the physical parameters involved.

References

[1] Alves C J S and Kress R 2002 On the far-field operator in elastic obstacle scattering *IMA J. Appl. Math.* **67** 1–21

[2] Arens T 2001 Linear sampling methods for 2D inverse elastic wave scattering *Inverse Problems* **17** 1445–64

[3] Arens T and Grinberg N I 2005 A complete factorization method for scattering by periodic surfaces *Computing* **75** 111–32

[4] Arens T and Kirsch A 2003 The factorization method in inverse scattering from periodic structures *Inverse Problems* **19** 1195–211

[5] Atkinson K E 1997 *The Numerical Solution of Integral Equations of the Second Kind* (Cambridge: Cambridge University Press)

[6] Bal G 2005 Reconstructions in impedance and optical tomography with singular interfaces *Inverse Problems* **21** 113–31

[7] Billingham J and King A C 1997 *Wave Motion* (*Cambridge Texts in Applied Mathematics* vol 24) (New York: Cambridge University Press)

[8] Brühl M 2001 Explicit characterization of inclusions in electrical impedance tomography *SIAM J. Math. Anal.* **32** 1327–41

[9] Brühl M and Hanke M 2000 Numerical implementation of two noniterative methods for locating inclusions by impedance tomography *Inverse Problems* **16** 1029–42

[10] Cakoni F and Colton D 2006 *Qualitative Methods in Inverse Scattering Theory* (Berlin: Springer-Verlag)

[11] Cakoni F, Colton D and Haddar H 2002 The linear sampling method for anisotropic media *J. Comput. Appl. Math.* **146** 285–99

[12] Cakoni F and Haddar H 2012 Transmission Eigenvalues in Inverse Scattering Theory *Inside Out II* ed G Uhlmann (MSRI Publications) vol 60 pp 527–78

[13] Charalambopoulos A, Kirsch A, Anagnostopoulos K A, Gintides D and Kiriaki K 2007 The factorization method in inverse elastic scattering from penetrable bodies *Inverse Problems* **23** 27–51

[14] Colton D, Giebermann K and Monk P 2000 A regularized sampling method for solving three dimensional inverse scattering problems *SIAM J. Sci. Comput.* **21** 2316–30

[15] Colton D and Kress R 1983 *Integral Equation Methods in Scattering Theory* (New York: Wiley-Interscience)

[16] Colton D and Kress R 1998 *Inverse Acoustic and Electromagnetic Scattering Theory* 2nd edn (Berlin: Springer-Verlag)

[17] Colton D and Kress R 2006 Using fundamental solutions in inverse scattering *Inverse Problems* **22** R49–R66

[18] Costabel M and Stephan E 1985 A direct boundary integral equation method for transmission problems *J. Math. Anal. Appl.* **106** 367–413

[19] Gebauer B 2006 The factorization method for real elliptic problems *Z. Anal. Anwendungen* **25** 81–102

[20] Gebauer B, Hanke M, Kirsch A, Muniz W and Schneider C 2005 A sampling method for detecting buried objects using electromagnetic scattering *Inverse Problems* **21** 2035–50

[21] Grinberg N I 2006 The operator factorization method in inverse obstacle scattering *Integral Equations Operator Theory* **54** 333–48

[22] Grinberg N I and Kirsch A 2004 The factorization method for obstacles with a-priori separated sound-soft and sound-hard parts *Math. Comput. Simulation* **66** 267–79

[23] Hähner P 1999 An inverse problem in electrostatics *Inverse Problems* **15** 961–75

[24] Hanke M and Brühl M 2003 Recent progress in electrical impedance tomography *Inverse Problems* **19** S65–S90

[25] Hyvönen N 2005 Application of a weaker formulation of the factorization method to the characterization of absorbing inclusions in optical tomography *Inverse Problems* **21** 1331–43

[26] Kirsch A 1989 Surface gradients and continuity properties for some integral operators in classical scattering theory *Math. Method Appl. Sci.* **11** 789–804

[27] Kirsch A 1996 *An Introduction to the Mathematical Theory of Inverse Problems* (*Applied Mathematical Sciences* vol 120) (Berlin: Springer-Verlag)

[28] Kirsch A 1998 Characterization of the shape of a scattering obstacle using the spectral data of the far-field operator *Inverse Problems* **14** 1489–512

[29] Kirsch A 1999 Factorization of the far-field operator for the inhomogeneous medium case and an application in inverse scattering theory *Inverse Problems* **15** 413–29

[30] Kirsch A 2000 New characterization of solutions in inverse scattering theory *Appl. Anal.* **76** 319–50

[31] Kirsch A 2002 The MUSIC algorithm and the factorization method in inverse scattering theory for inhomogeneous media *Inverse Problems* **18** 1025–40

[32] Kirsch A 2004 The factorization method for Maxwell's equations *Inverse Problems* **20** S117–S134

[33] Kirsch A 2005 The factorization method for a class of inverse elliptic problems *Math. Nachr.* **278** 258–77

[34] Kirsch A and Grinberg N 2008 *The Factorization Method for Inverse Problems* (*Oxford Lecture Series in Mathematics and its Applications* vol 36) (Oxford: Oxford University Press)

[35] Kirsch A and Kleefeld A 2012 The factorization method for a conductive boundary condition *J. Integral Equations Appl.* **24** 575–601

[36] Kirsch A and Kress R 1993 Uniqueness in inverse obstacle scattering *Inverse Problems* **9** 285–99

[37] Kirsch A and Liu X 2013 The factorization method for inverse acoustic scattering by a penetrable anisotropic obstacle *Math. Method Appl. Sci.* doi: `http://dx.doi.org/10.1002/mma.2877`

[38] Kirsch A and Ritter S 2000 A linear sampling method for inverse scattering from an open arc *Inverse Problems* **16** 89–105

[39] Kleefeld A 2009 *Direct and inverse acoustic scattering for three-dimensional surfaces* Ph.D. Thesis, University of Wisconsin – Milwaukee

[40] Kleefeld A 2012 The exterior problem for the Helmholtz equation with mixed boundary conditions in three dimensions *Int. J. Comput. Math.* **89** 2392–409

[41] Kleefeld A 2012 A modified boundary integral equation for solving the exterior Robin problem for the Helmholtz equation in three dimensions *Appl. Math. Comput.* **219** 2114–23

[42] Kleefeld A 2012 The transmission problem for the Helmholtz equation in $\mathbb{R}^3$ *Comput. Methods Appl. Math.* **12** 330–50

[43] Kleefeld A and Lin T-C 2011 The nonlinear Landweber method applied to an inverse scattering problem for sound-soft obstacles in 3D *Comput. Phys. Comm.* **182** 2550–60

[44] Kleefeld A and Lin T-C 2012 Boundary element collocation method for solving the exterior Neumann problem for Helmholtz's equation in three dimensions *Electron. Trans. Numer. Anal.* **39** 113–43

[45] Kleinman R E and Martin P A 1998 On single integral equations for the transmission problem in acoustics *SIAM J. Appl. Math.* **48** 307–25

[46] Kress R 2002 A sampling method for an inverse boundary value problem for harmonic vector fields *Ill-Posed and Inverse Problems* ed S Kabanikhin and V G Romanov (Utrecht: VSP) pp 243–62

[47] Kress R 2003 A factorization method for an inverse Neumann problem for harmonic vector fields *Georgian Math. J.* **10** 549–60

[48] Kress R and and Kühn L 2002 Linear sampling methods for inverse boundary value problems in potential theory *Appl. Numer. Math.* **43** 161–73

[49] McLean W 2000 *Strongly Elliptic Systems and Boundary Integral Equations* (Cambridge: Cambridge University Press)

[50] Morozov V A 1984 *Methods for Solving Incorrectly Posed Problems* (New York: Springer-Verlag)

[51] Naylor A W and Sell G R 1982 *Linear Operator Theory in Engineering and Science, 2nd edition* (*Applied Mathematical Sciences* vol 40) (New York: Springer-Verlag)
[52] Potthast R 2005 Sampling and probe methods—an algorithmical view *Computing* **75** 215–35
[53] Potthast R 2006 A survey on sampling and probe methods for inverse problems *Inverse Problems* **22** R1–R47
[54] Tikhonov A N, Goncharsky A V, Stepanov V V and Yagola A G 1995 *Numerical Methods for the Solution of Ill-Posed Problems* (Dordrecht: Kluwer)